Original Article

Anti-ferroptotic *PRKAA2* serves as a potential diagnostic and prognostic marker for hepatoblastoma

Yi Xie[1,2#], Zhongqi Cui[3#], Sijia Fang[1,2], Guoqing Zhu[1,2], Ni Zhen[1,2], Jiabei Zhu[1,2], Siwei Mao[1,2], Fenyong Sun[3], Qiuhui Pan[1,2,4], Ji Ma[1,2]^

[1]Clinical Laboratory, Shanghai Children's Medical Center, School of Medicine, Shanghai Jiao Tong University, Shanghai, China; [2]Shanghai Key Laboratory of Clinical Molecular Diagnostics for Pediatrics, Shanghai, China; [3]Department of Clinical Laboratory Medicine, Shanghai Tenth People's Hospital of Tongji University, Shanghai, China; [4]Sanya Women and Children's Hospital Managed by Shanghai Children's Medical Center, Sanya, China

Contributions: (I) Conception and design: Y Xie, Z Cui, Q Pan, J Ma; (II) Administrative support: F Sun, J Ma, Q Pan; (III) Provision of study materials or patients: Y Xie, Z Cui, Q Pan, J Ma; (IV) Collection and assembly of data: G Zhu, Y Xie, S Fang; (V) Data analysis and interpretation: Y Xie, S Fang, S Mao, J Zhu, N Zhen; (VI) Manuscript writing: All authors; (VII) Final approval of manuscript: All authors.

[#]These authors contributed equally to this work.

Correspondence to: Qiuhui Pan, MD, PhD. Clinical Laboratory, Shanghai Children's Medical Center, School of Medicine, Shanghai Jiao Tong University, 1678 Dongfang Road, Shanghai 200127, China; Shanghai Key Laboratory of Clinical Molecular Diagnostics for Pediatrics, Shanghai 200127, China; Sanya Women and Children's Hospital Managed by Shanghai Children's Medical Center, Sanya 572000, China. Email: panqiuhui_med@163.com; Ji Ma, PhD. Clinical Laboratory, Shanghai Children's Medical Center, School of Medicine, Shanghai Jiao Tong University, 1678 Dongfang Road, Shanghai 200127, China; Shanghai Key Laboratory of Clinical Molecular Diagnostics for Pediatrics, Shanghai 200127, China. Email: maji@scmc.com.cn.

Background: The incidence rate of hepatoblastoma (HB), which is the most prevalent malignant tumour among children, rises each year. According to recent studies, a number of neoplastic disorders and ferroptosis are intimately connected. This study aims to identify key ferroptosis-related genes in HB and explore new directions for the diagnosis and treatment of HB.

Methods: Differentially expressed ferroptosis-related genes were identified using the Gene Expression Omnibus datasets. The functional annotation of candidate genes was evaluated through Gene Ontology (GO) and Kyoto Encyclopedia of Genes and Genomes (KEGG) pathway analyses. Machine learning and receiver operating characteristic (ROC) curves revealed protein kinase AMP-activated catalytic subunit alpha 2 (*PRKAA2*), tribbles homolog 2 (*TRIB2*), and liver-type glutaminase (*GLS2*) as potential diagnostic genes of HB. By using quantitative reverse transcription polymerase chain reaction (qRT-PCR) and immunohistochemistry, relative expression of *PRKAA2* was examined. The effect of *PRKAA2* on proliferation, apoptosis, and ferroptosis of HB cells was verified *in vitro* and *in vivo*. Fisher's exact test was used to evaluate the clinical significance of *PRKAA2* in HB.

Results: The prognostic indicators had a substantial correlation with *PRKAA2* expression, which rose dramatically in HB tissues. *PRKAA2* promotes proliferation and inhibits ferroptosis in HB cells. *PRKAA2* plays a role in ferroptosis by regulating hypoxia-inducible factor 1α (*HIF-1α*) and transferrin receptor 1 (*TFR1*).

Conclusions: *PRKAA2* functions as a tumor-promoting factor in HB by promoting cell proliferation and prohibiting ferroptosis. Ferroptosis-related genes *PRKAA2* is a potential diagnostic and prognostic marker for HB as well as a novel therapeutic target in the future.

Keywords: Hepatoblastoma; ferroptosis; prognostic signature; biomarker; gene expression omnibus database

^ ORCID: 0000-0001-6904-5360.

Submitted Feb 11, 2023. Accepted for publication Jul 18, 2023. Published online Aug 11, 2023.
doi: 10.21037/jgo-23-110
View this article at: https://dx.doi.org/10.21037/jgo-23-110

Introduction

Hepatoblastoma (HB), an embryonic tumor caused by the abnormal development of liver blastocytes, accounts for ~80% of primary liver malignant tumors in children (1). The annual incidence of HB is about 0.5–1.5/1 million (2), and the incidence is increasing in recent years (3). HB has an insidious onset with rapid progression; most patients are asymptomatic in the early stage. Most patients with HB are diagnosed with abdominal mass accompanied by elevated alpha-fetoprotein (AFP) levels. Effective biomarkers for the diagnosis of HB are lacking, and serum AFP level remains the most important diagnostic and monitoring marker of HB in the clinic (4). However, elevated AFP level is common in benign liver lesions and healthy infants and reduced AFP level occurs in 5–10% of patients with HB (5). This suggests that AFP has a limited role as a biomarker of HB. Complete tumor resection is the main method for treating HB and reducing recurrence (6), but most children cannot undergo radical resection because of the huge liver mass at diagnosis (7). Therefore, understanding the molecular mechanism of HB pathogenesis and identifying effective biomarkers will help in the early diagnosis of HB, development of treatment methods for HB, and improving the prognosis in children with HB.

Ferroptosis, characterized by changes in cellular metabolism in response to the environment, is a type of programmed cell death. Reactive oxygen species (ROS) and polyunsaturated fatty acids are created in high quantities during ferroptosis, leading to phospholipid peroxidation (8,9). It has been claimed that ferroptosis has a role in the occurrence and progression of plenty of diseases in human. Additionally, it has been shown that ferroptosis functions as a tumour suppression mechanism and is connected to the pathophysiology of a number of tumors (10). Iron, amino acids, glutathione (GSH), ROS and lipid peroxidation (LPO) metabolism are all involved in ferroptosis. In 2015, Gao *et al.* demonstrated that glutamate, glutamine, and transferrin are key regulators of ferroptosis (11). Since then, many studies have shown that several genes and proteins play a role in ferroptosis. Some molecules have a direct or indirect impact on ferroptosis, such as glutathione peroxidase 4 (*GPX4*) (12), nuclear factor E2-related factor 2 (*NRF2*) (13), tumor suppressor P53 (*TP53*) (14), heat shock protein B1 (15), NADPH oxidase (16) and solute carrier family 7 member 1 (*SLC7A11*) (17). However, studies on ferroptosis in HB are limited, and the role of ferroptosis in HB pathogenesis is unclear. Studies on ferroptosis-related markers in HB may help with HB diagnosis and therapy.

In this work, key ferroptosis-related genes (FRGs) in HB were identified to tackle the issue of lacking of biomarkers. Protein kinase AMP-activated catalytic subunit alpha 2 (*PRKAA2*), tribbles homolog 2 (*TRIB2*), and liver-type glutaminase (*GLS2*) were identified from differentially expressed FRGs (DE-FRGs) in patients with HB. *PRKAA2* was selected for functional verification in HB cell lines and *in vivo*, and the role of *PRKAA2* in ferroptosis was preliminarily evaluated. We present this article in accordance with the ARRIVE reporting checklist (available at https://jgo.amegroups.com/article/view/10.21037/jgo-23-110/rc).

Highlight box

Key findings

- PRKAA2 functions as a tumor-promoting factor in hepatoblastoma and is a potential diagnostic and prognostic marker for hepatoblastoma.

What is known and what is new?

- Ferroptosis is known to play a key role in the development of tumor.
- The clinical value of PRKAA2 for hepatoblastoma was analyzed for the first time. We investigated further the mechanism by which PRKAA2 regulates ferroptosis.

What is the implication, and what should change now?

- An adequate understanding of the relationship between PRKAA2 and ferroptosis can contribute to diagnosis and therapeutic strategy of hepatoblastoma.

Methods

The HB dataset

The Gene Expression Omnibus database portal is where the GSE131329 and GSE75271 files were downloaded. GSE131329, which contains 53 HB samples and fourteen

noncancerous liver samples, underwent analysis with the GPL6244 platform, whereas GSE75271, which includes 50 HB samples and five noncancerous liver samples, underwent analysis with the GPL570 platform.

DE-FRGs determination and integrated microarray dataset analyses

Using "limma" in R, differentially expressed genes (DEGs) between tumor and non-tumor liver samples were identified. $|Log_2FC|>1$, $P<0.05$, and false discovery rate (FDR) <0.05 were thresholds for DEGs (18). GSE131329 and GSE75271 were analyzed separately and the intersection was taken. 29 DE-FRGs were identified by searching the ferroptosis-related database FerrDb (19). Visualisation was conducted using a heatmap by R package "pheatmap".

Functional annotation and enrichment analyses

To evaluate the functional annotation of candidate genes, Gene Ontology (GO) and Kyoto Encyclopedia of Genes and Genomes (KEGG) pathway analyses were completed using "clusterProfiler" in R (20). All genes were encoded by GO terms and KEGG pathways and analyzed by computational methods. GO terms included biological process, cellular component and molecular function. The P value was corrected using the Benjamini method for multiple testing calibrations. Adjusted $P<0.05$ were considered significantly enriched. The results were visualised by the R package "ggplot2".

Selection of potential diagnostic markers

Two machine learning methods for predicting HB status were employed to find potential diagnostic factors. LASSO (least absolute shrinkage and selection operator) is a regression analytical arithmetic that performs regularization to increase prediction accuracy. The "glmnet" package in R was used to conduct LASSO regression analysis to identify the genes substantially associated with the ability of HB and noncancerous liver samples to distinguish one another. Then binomial distribution variables were used and a minimum criterion of standard error value is added to establish the model. Support vector machine (SVM) is a supervised machine learning method, to avoid overfit, recursive feature elimination (RFE) was used to identify optimum genes from the metadata cohort. Hence, SVM-RFE was used to identify the gene set with the greatest discrimination ability. Receiver operating characteristic (ROC) curves and area under the ROC curve (AUC) were generated using the R package "pROC" to investigate the categorizing impacts of the major genes on HB and noncancerous liver specimens.

CIBERSORT analysis

A deconvolution technique based on gene expression profiles is utilized in the computational approach of CIBERSORT (http://cibersort.stanford.edu/), which is used to evaluate changes in a gene group in relation to the other genes in a sample. In noncancerous liver samples and HB samples, CIBERSORT was utilized to determine the immunological responses of 22 immune cells and assess the relationship between the immune cells and the level of important genes. A "signature matrix" of barcode genes that are enriched in each target cell type is needed as input for CIBERSORT. There should be no missing data and all gene expression levels should be in non-log space with positive numbers (21). Upload the correctly formatted mixture file to the website. Then run CIBERSORT and select "LM22 (22 immune cell types)".

Patients and paired tissue collections

30 pairs of HB samples and adjacent noncancerous samples were collected from patients who underwent HB surgery at Shanghai Children's Medical Center from September 2019 to June 2022. This study was approved by the Institutional Research Ethical Committee of Shanghai Children's Medical Centre (No. SCMCIRB-K2021076-1, 2021.10.10). All patients or their guardians provided their verbal and written consent. The study was conducted in accordance with the Declaration of Helsinki (as revised in 2013).

RNA extraction and quantitative reverse transcription polymerase chain reaction (qRT-PCR) analysis

TRIzol reagent (15596018, Invitrogen, Thermo Scientific, Shanghai, China) was used to separate the total RNA from the HB tissue and HB cell lines. Total mRNA was reverse-transcribed into cDNA with the prime script Reverse Transcription reagent kit (RR047, TaKaRa Bio, Shiga, Japan). SYBR Green reagent kit (RR820, TaKaRa Bio, Shiga, Japan) was used to determine the relative expression of mRNA in an ABI 7500 PCR system (Applied Biosystems, Forster City, California, USA). The $2^{-\Delta\Delta CT}$ method was

applied for relative quantitation. As an internal control, 18s rRNA was employed. In the Appendix 1, the primers are provided. Correlation analysis was performed using the ΔΔCT method (22).

Immunohistochemistry

Sections that were embedded in paraffin were deparaffinized with xylene and hydrated using an ethanol gradient. The slices were then transferred to a 10 mmol/L sodium citrate solution for antigen recovery after being treated in 3% methanol-H_2O_2. The sections were incubated with anti-PRKAA2 antibodies (1/100; Proteintech, 18167-1-AP, RRID:AB_10695046), followed by secondary antibodies (1/1,000; Abcam, ab7090, RRID:AB_955417), after being blocked with 5% skimmed milk powder solution at 25 ℃. Color was developed using DAB (3,3N-Diaminobenzidine Tertrahydrochloride), and the film was mounted with neutral gum.

Cell culture, transient transfection and lentivirus transduction

The Cell bank of Chinese Academy of Science (Shanghai, China) provided the HepG2 (RRID: CVCL_1×10), HUH6 (RRID: CVCL_4381) and HEK293T (RRID: CVCL_0063) cells. THLE-2 (RRID: CVCL_3803) was obtained from Ningbo Mingzhou Biotechnology Co., Ltd. (Ningbo, China). HepG2 cells were cultured in minimum Eagle's medium (MEM) (SH30265.01, HyClone, Logan, UT, USA), HUH6 and HEK293T cells were cultured in Dulbecco's modified Eagle's medium (DMEM) (C11995500BT, Gibco Laboratories), and BEBM medium (CC3170, Lonza/Clonetics Corporation, Walkersville, MD, USA) was employed to culture THLE-2 cells. All cells were cultured with 10% fetal bovine serum (FBS) and 1% antibiotic (Gibco, Carlsbad, CA, USA). Specifically, BEBM medium was supplemented with 5 μg/L EGF (SRP3027, Sigma-Aldrich) and 70 μg/L phosphorylethanolamine (HY-N5034, MedChemExpress, Monmouth Junction, NJ, USA). All cultures were kept alive at 37 ℃ in an incubator with 5% CO_2 humidity (Thermo Fisher Scientific, Waltham, MA, USA). Prior to the transfection day, 2.5×10^5/mL of HepG2 and HUH6 cells were planted in six-well plates and cultured for an overnight period at 40–60% confluence. Lipofectamine 2000 (11668019, Invitrogen, Carlsbad, CA, USA) has been employed to transfect these cells with siRNA targeted against *PRKAA2* (GenePharma, Shanghai, China). The cells were then incubated for 48 hours. Target sequences are listed in Appendix 1. For lentivirus transduction, the plasmids and a packaging plasmid were transfected into HEK293T cells; 48 h later, supernatants were obtained and utilized to infect HB cells for 48 h. Finally, HB cells were cultured in the company of 2 mg/L puromycin to obtain stable cell lines.

Western blotting assay

RIPA lysis buffer (P0013B, Beyotime, Jiangsu, China) mixed with phosphatase and protease inhibitors (P1046, Beyotime, Jiangsu, China) was used to lyse the cells on ice. Afterwards, sodium dodecyl sulfate (SDS) was added to the total protein after it had been measured. Then, 40 μg of protein was transferred to nitrocellulose membranes (HATF85R, Millipore, Bedford, MA, USA) after being separated on SDS polyacrylamide gel electrophoresis. The membranes were then blocked and treated with primary antibodies at 4 ℃ for an overnight period. The membranes were then cleaned and treated with secondary antibodies that had been colored fluorescently (Licor, USA). Finally, an Odyssey equipment (Licor, USA) was used to see the bands on the membranes. The Appendix 1 contains a collection of information about primary antibodies.

Cell proliferation and colony formation assay

Cell counting kit-8 (CCK8) reagent (C0043, Beyotime, Jiangsu, China) was used to measure cell viability. Briefly, the specified treatments were applied to the cells after they were seeded into 96-well plates. Following this, 100 μL of fresh medium containing 10 μL of CCK8 solutions were added to cells. Then the cells were cultured for 2 hours (37 ℃, 5% CO_2). Afterwards, the absorbance was spectrophotometrically measured at 450 nm. Both the relative cell viability and the collected data were normalized to the corresponding dimethyl sulphoxide-treated wells. Cells (500 cells/well) were sown in six-well plates for colony formation assay and cultured for 1–2 weeks until the emergence of cell colonies. These colonies were then preserved with methanol and stained with Giemsa.

Cell apoptosis analysis

After transfection, 5×10^5 *PRKAA2* knockdown cells were collected and washed. After that, cells were stained for 10 minutes with Annexin V that had been fluorescein

isothiocyanate-conjugated (C1062M-1, Beyotime, Jiangsu, China), and then for 10 minutes with Propidium Iodide (PI) (C1062M-3, Beyotime, Jiangsu, China). A FACSCanto II flow cytometer (BD, New Jersey, USA) was then used to calculated the proportion of apototic cells.

Xenograft tumor assay

Experiments were performed under a project license (No. SYXK2019-0025, 2022.4.22) granted by the Shanghai Children's Medical Center, in compliance with institutional guidelines for the care and use of animals. The nude mice were provided by Shanghai Laboratory Animal Center and kept in SPF animal feeding room of Shanghai Children's Medical Center. The physiological habits of nude mice were fully taken into account in the building of the feeding room, with humidity of 50–60% and temperature of 24 ℃. The daily diet of nude mice was uniformly fed and managed by professionals. A xenograft tumor model was established by subcutaneous injection of 4-week-old male nude mice with 1×10^7 cells. The same batch of mice were purchased and randomly selected for vaccination. Each group contained five mice and the mice were marked with scissor toe. After 25 days, the mice were sacrificed by spinal dislocation and the tumors were weighed. If the nude mice died or became seriously ill during the period, they were not included in the statistics.

Lipid ROS assay

The cells were plated in a six-well plate and incubated with 5 μM BODIPY-C11 (D3861, Thermo Fisher Scientific) for 30 minutes (37 ℃, 5% CO_2), which was added to the culture media. Using trypsin without ethylene diamine tetraacetie acid, the cells were collected, followed by two phosphate buffered saline (PBS) washes and resuspension in 500 μL PBS. The CytoFLEX cytometer (Beckman Coulter, California, USA) was used to measured ROS levels, and the CytExpert software (Beckman Coulter, California, USA) was used to interpret the results.

Malondialdehyde (MDA), iron and GSH/glutathione oxidized (GSSG) assay

Assessment of the MDA concentration was completed using lipid peroxidation assay kit (ab118970, Abcam, Shanghai, China). GSH and GSSG assay kits (RK05819, ABclonal, Wuhan, China) were used to measure the GSH/GSSG ratio. The determination of intracellular iron level used the iron assay kit (ab83366, Abcam).

Reagents and the concentrations used

From Selleck Chemicals (Houston, Texas, USA), ferrostatin-1 (S7243), Z-VAD-FMK (S7023), and necrosulfonamide (S8251) were bought. HIF-1α-IN-2 (HY-115903) was purchased from MedChemExpress (New Jersey, USA). The concentrations of the stimuli were ferrostatin-1 (2 μM), Z-VAD-FMK (10 μM), necrosulfonamide (0.5 μM), HIF-1α-IN-2 (1 μM).

Statistical analysis

In this study, R software (version 4.0.1), SPSS software (version 24.0), or GraphPad Prism 8 were all used for all statistical analyses. Continuous variables were compared using the Pearson test. The means of two groups were compared using Student's *t*-tests. Comparative data between the three groups were compared using one-way analysis of variance. The correlation of *PRKAA2* expression and the clinicopathological characteristics of HB patients was examined using Fisher's exact test. The mean ± standard deviation (mean ± SD) from three independent experiments are used to represent all quantitative data. Unless otherwise stated, a significant difference was considered statistically when $P<0.05$.

Results

DE-FRGs in HB and functional enrichment analysis

Data from 103 patients with HB and nineteen controls from the GSE131329 (23) and GSE75271 (24) datasets were evaluated retrospectively. As described in the two articles (23,24), tumor samples and noncancerous liver samples were obtained before treatment. DEGs from source data were evaluated using "limma" in R. Then a total of 29 DE-FRGs were identified by searching FerrDb database, of which thirteen were up- and sixteen were downregulated significantly. The expression of 29 DE-FRGs in 103 HB samples compared with that in nineteen controls were shown by the heatmap (*Figure 1A*). We also performed correlation analysis between these 29 genes. $P<0.05$ were considered significantly correlate, r value >0 denotes a positive correlation while a r value <0 denotes a negative correlation (*Figure 1B*). The findings demonstrated that

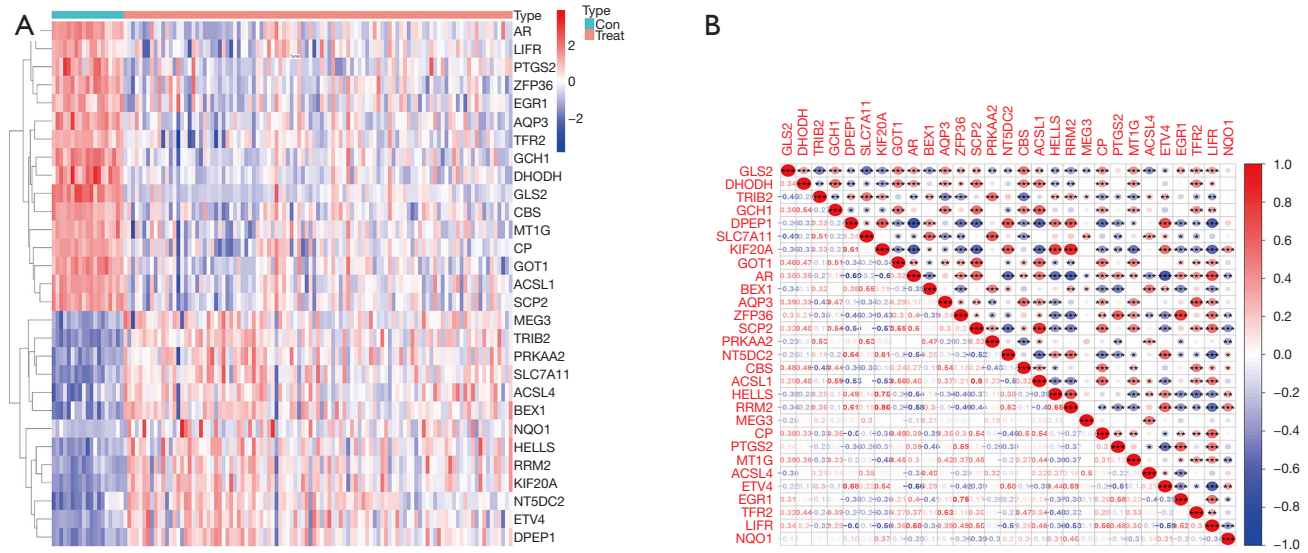

Figure 1 DE-FRGs in patients with HB. (A) Heatmap of expression of DE-FRGs in HB samples and noncancerous liver samples. 29 DE-FRGs were identified using "limma" in R. Each column represents a sample, and each row represents a DE-FRG. The gradual colour change from red to blue indicates the changing process from upregulation to downregulation. (B) Correlation analysis of 29 DE-FRGs expression by Spearman rank test. Each column and row represent a DE-FRG. *, P<0.05, **, P<0.01, and ***, P<0.001. r values are presented numerically, with >0 indicating a positive correlation and <0 indicating a negative correlation. DE-FRGs, differentially expressed ferroptosis-related genes; HB, hepatoblastoma.

there is dysregulation of ferroptosis-related genes in HB, which may be a key factor in the development of HB.

Discovering the connections between fundamental functions or pathways with genes of interest will enhance our understanding of their roles. To study the biological function of the screened FRGs in HB, GO analysis and KEGG analysis were carried out via "clusterProfiler" in R. The results revealed that DE-FRGs mainly participated in biological process, especially response to metal ion, response to nutrient levels and cellular response to metal ion, and were less involved in molecular function and cellular component. KEGG analysis revealed that arginine biosynthesis, ferroptosis, and fatty acid biosynthesis were significantly enriched. Thus, these genes may influence disease progression through lipid metabolism and ferroptosis. Details of the results of GO analysis and KEGG analysis are in *Tables 1*,*2*.

Expression and diagnosis significance of PRKAA2, TRIB2, and GLS2 in HB

Two algorithms were used to select the biomarkers of HB. DE-FRGs were identified using LASSO regression (*25*), The logistic LASSO regression includes HB as the dependent variable Y, coded 0 for samples without HB, 1 represents samples with HB. The punishment term lambda (λ) was chosen using ten-fold cross-validation. To gauge how well the fitted model performed predictions, binomial deviation was utilized. Eleven variables were identified as diagnostic markers of HB, including *GLS2*, dihydroorotate dehydrogenase (*DHODH*), *TRIB2*, GTP cyclohydrolase 1 (*GCH1*), aquaporin 3 (*AQP3*), *PRKAA2*, 5'-nucleotidase domain containing 2 (*NT5DC2*), prostaglandin-endoperoxide synthase 2 (*PTGS2*), metallothionein 1G (*MT1G*), LIF receptor subunit alpha (*LIFR*) and NAD(P)H quinone dehydrogenase 1 (*NQO1*) (Figure S1A,S1B). SVM-RFE is a process that involves iteratively removing features in a backward manner. The process continues until there is only one feature left, providing a list of features in order of importance. During the algorithm, features with the lowest ranking weight are removed, while retaining significant feature variables. Analysis using the SVM-RFE algorithm (*26*) revealed four subsets of features, including *TRIB2*, *GLS2*, *PRKAA2* and dipeptidase 1 (*DPEP1*) (Figure S1C,S1D). Finally, to identify the most valuable DE-FRGs three overlapping features (*PRKAA2*, *TRIB2*, and *GLS2*) were selected between the two algorithms, indicating that these three genes play important roles in HB

Table 1 Results of GO analysis

Module	GO_ID	GO_Term	Count	P value	Genes
BP	GO:0010038	Response to metal ion	8	5.59×10^{-8}	*DPEP1/GOT1/AQP3/PRKAA2/PTGS2/MT1G/TFR2/NQO1*
	GO:0031667	Response to nutrient levels	8	3.97×10^{-7}	*DHODH/AQP3/ZFP36/PRKAA2/ACSL1/PTGS2/ACSL4/NQO1*
	GO:0071248	Cellular response to metal ion	6	4.14×10^{-7}	*DPEP1/PRKAA2/PTGS2/MT1G/TFR2/NQO1*
	GO:0071241	Cellular response to inorganic substance	6	9.16×10^{-7}	*DPEP1/PRKAA2/PTGS2/MT1G/TFR2/NQO1*
	GO:0046394	Carboxylic acid biosynthetic process	7	1.07×10^{-6}	*GLS2/GCH1/GOT1/SCP2/PRKAA2/CBS/PTGS2*
	GO:0016053	Organic acid biosynthetic process	7	1.09×10^{-6}	*GLS2/GCH1/GOT1/SCP2/PRKAA2/CBS/PTGS2*
CC	GO:0005777	Peroxisome	3	0.00087	*SCP2/ACSL1/ACSL4*
	GO:0042579	Microbody	3	0.00087	*SCP2/ACSL1/ACSL4*
	GO:0005778	Peroxisomal membrane	2	0.0031	*ACSL1/ACSL4*
	GO:0031903	Microbody membrane	2	0.0031	*ACSL1/ACSL4*
	GO:0031968	Organelle outer membrane	3	0.0032	*ACSL1/PTGS2/ACSL4*
	GO:0019867	Outer membrane	3	0.0033	*ACSL1/PTGS2/ACSL4*
MF	GO:0102391	Decanoate-CoA ligase activity	2	0.0070	*ACSL1/ACSL4*
	GO:0031956	MMedium-chain fatty acid-CoA ligase activity	2	0.0070	*ACSL1/ACSL4*
	GO:0047676	Arachidonate-CoA ligase activity	2	0.0070	*ACSL1/ACSL4*
	GO:0004467	Long-chain fatty acid-CoA ligase activity	2	0.0074	*ACSL1/ACSL4*
	GO:0003996	Acyl-CoA ligase activity	2	0.0091	*ACSL1/ACSL4*
	GO:0015645	Fatty acid ligase activity	2	0.015	*ACSL1/ACSL4*

GO, Gene Ontology; BP, biological process; CC, cellular component; MF, molecular function.

Table 2 Results of KEGG analysis

Pathway ID	Pathway term	Count	P value	Genes
hsa04216	Ferroptosis	4	3.08×10^{-6}	*SLC7A11/ACSL1/CP/ACSL4*
hsa01212	Fatty acid metabolism	3	0.00039	*SCP2/ACSL1/ACSL4*
hsa04920	Adipocytokine signaling pathway	3	0.00069	*PRKAA2/ACSL1/ACSL4*
hsa03320	PPAR signaling pathway	3	0.00088	*SCP2/ACSL1/ACSL4*
hsa00061	Fatty acid biosynthesis	2	0.00094	*ACSL1/ACSL4*
hsa04146	Peroxisome	3	0.0011	*SCP2/ACSL1/ACSL4*
hsa00220	Arginine biosynthesis	2	0.0014	*GLS2/GOT1*
hsa00250	Alanine, aspartate and glutamate metabolism	2	0.0040	*GLS2/GOT1*
hsa00071	Fatty acid degradation	2	0.005	*ACSL1/ACSL4*
hsa01240	Biosynthesis of cofactors	3	0.0067	*DHODH/GCH1/NQO1*
hsa00270	Cysteine and methionine metabolism	2	0.0074	*GOT1/CBS*

KEGG, Kyoto Encyclopedia of Genes and Genomes.

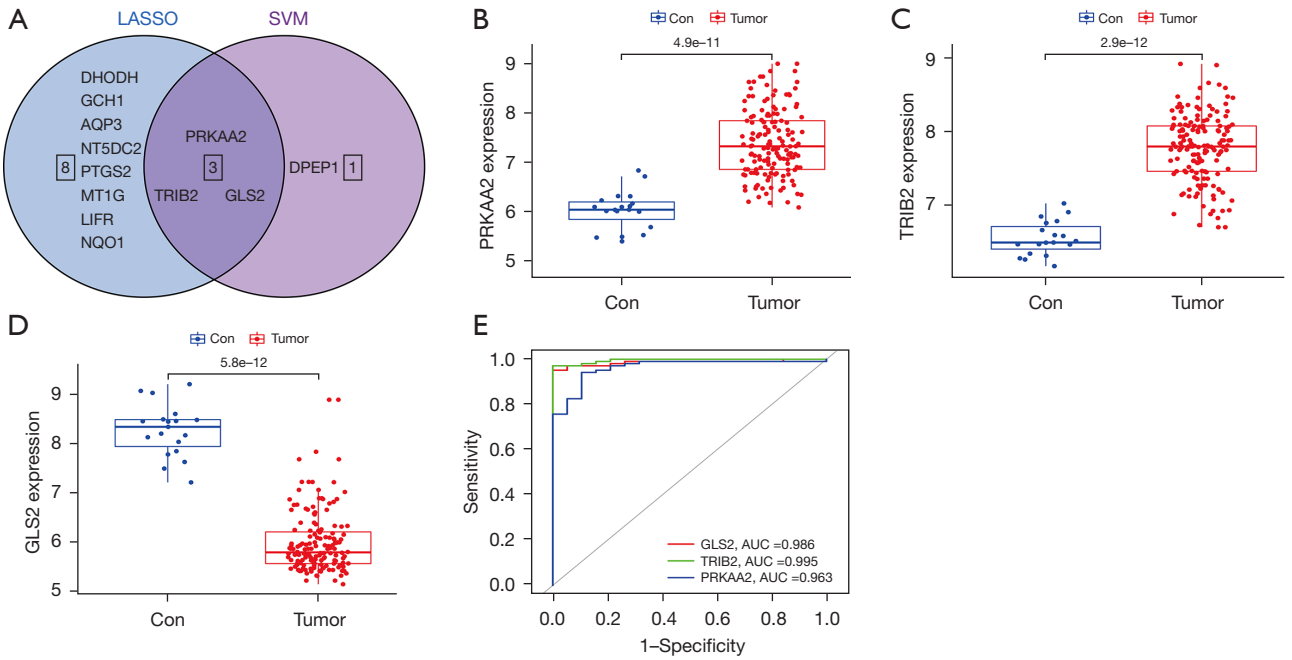

Figure 2 Diagnosis marker candidates for HB. (A) Venn graph displaying the three biomarkers for diagnosis that both LASSO and SVM-RFE share. The overlap contains three genes: *PRKAA2*, *TRIB2* and *GLS2*. (B) The expression of *PRKAA2* was considerably increased in HB samples (P=4.9e−11 by *t*-test). (C) The expression of *TRIB2* was considerably increased in HB samples (P=2.9e−12 by *t*-test). (D) *GLS2* expression was distinctly downregulated in HB samples (P=5.8e−12 by *t*-test). (E) ROC curves assays for *PRKAA2*, *TRIB2*, and *GLS2* in HB via the R package "pROC". HB, hepatoblastoma; LASSO, least absolute shrinkage and selection operator; SVM-REF, support vector machine recursive feature elimination; ROC, Receiver operating characteristic; AUC, area under the curve; PRKAA2, protein kinase AMP-activated catalytic subunit alpha 2; TRIB2, tribbles homolog 2; GLS2, liver-type glutaminase.

development (*Figure 2A*).

The expression of *GLS2* was significantly lower (*Figure 2B*) and that of *PRKAA2* and *TRIB2* was significantly higher (*Figure 2C,2D*) in HB samples than in noncancerous liver samples. To further assess the diagnostic utility of *PRKAA2*, *TRIB2*, and *GLS2*, ROC assays were carried out. ROC curves and AUC were computed using "pROC" in R. When screening HB samples from noncancerous liver samples, the three genes shown a good competence. AUC values for *PRKAA2*, *TRIB2*, and *GLS2* were 0.963 (95% CI: 0.942–0.985), 0.995 (95% CI: 0.971–1.000), and 0.986 (95% CI: 0.951–1.000), respectively (*Figure 2E*).

PRKAA2 is a potential prognostic marker for HB

The infiltration of immune cells in the tumor microenvironment is an independent predictor of prognosis. In recent years, ferroptosis and immunity have been revealed to interact extremely closely by a number of studies, with this relationship being critical to the development, progression, and treatment of many malignancies (27-32). Therefore, the status of immune cell infiltration in HB and noncancerous liver samples was evaluated. The CIBERSORT method was employed to calculate the proportion of 22 types of infiltrating immune cells in tissues to evaluate the characteristics of immune cells. Six types of immune cells showed an imbalance between noncancerous liver samples and HB samples. Compared with controls, tumor tissues generally contained a lower fraction of T cells regulatory, NK cells resting, dendritic cells activated and neutrophils and a higher fraction of macrophages M0, and mast cells resting (Figure S2A).

The degree of immune infiltration was examined with the expression of *PRKAA2*, *TRIB2*, and *GLS2*. *PRKAA2* mRNA expression is positively correlated with macrophages M1 and mast cell resting and negatively correlated with neutrophils, macrophages M2 and mast cells activated. *TRIB2* mRNA expression is positively correlated with NK cells activated and negatively correlated with cells activated and neutrophils. *GLS2* mRNA expression is positively

correlated with B cells memory and neutrophils and negatively correlated with mast cells resting (Figure S2B). It can be concluded from the results that *PRKAA2*, *TRIB2* and *GLS2* were all correlated with immune cells.

PRKAA2 expression was evaluated in tumor tissues and paired adjacent noncancerous liver tissues from 30 patients with HB. Analysis using qRT-PCR and histochemistry revealed that *PRKAA2* expression was upregulated in HB samples (*Figure 3A*,*3B*). We also evaluated the expression of *TRIB2* and *GLS2* (Figure S3A-S3D), but there was no difference in the expression of TRIB2 protein between tumor tissue and noncancerous liver tissue. Moreover, we would like to choose genes that promote tumor and can be used as biomarkers and therapeutic targets for research, so *PRKAA2* was selected. As shown in *Table 3*, we collated the clinical information and pathological features of 30 patients with HB, including sex, age at diagnosis, AFP at diagnosis, AFP at final detection, tumor size, histology, PRETEXT (PRE-Treatment EXTent of tumor) stage and PRETEXT annotation factors such as metastasis, vascular involvement, tumor rupture, multifocality, extrahepatic spread and caudate involvement (33). According to the median value of ΔΔCt [ΔΔCt=ΔCt (normalized noncancerous) – ΔCt (normalized tumor)], the results of tissue samples determined using qRT-PCR are separated into *PRKAA2* low expression group and *PRKAA2* high expression group. The RNA level of *PRKAA2* was significantly correlated with PRETEXT stage of HB patients (P=0.021) (*Table 4*). According to the staining intensity of PRKAA2, tissue samples were separated into two groups: PRKAA2 low expression group (–, +) and PRKAA2 high expression group (++, +++). The protein level of PRKAA2 is significantly correlated with serum AFP level at the time of diagnosis (P=0.042), PRETEXT stage (P=0.007), distant metastasis (P=0.014) and multifocality (P=0.017) in HB patients (*Table 5*). These results suggest that *PRKAA2* expression can reflect the progress of HB and are significantly correlated with prognostic factors. Therefore, *PRKAA2* expression level may have the potential to be used for prognostic assessment of HB patients.

PRKAA2 plays a carcinogenic role in HB through ferroptosis

Comparing HB cells to normal cells, *PRKAA2* expression was likewise elevated (*Figure 3C*,*3D*). Then, *PRKAA2* was knocked down with small interfering RNAs (siRNA) and downregulation of *PRKAA2* was verified via western blot and qRT-PCR analysis (Figure S4A,S4B). Results from the CCK-8 assays showed that *PRKAA2* silencing significantly reduced the proliferation of both HepG2 and HUH6 cells (*Figure 3E*). Furthermore, interfering with *PRKAA2* expression inhibited colony formation (*Figure 3F*,*3G*). Results from flow cytometry analysis revealed that *PRKAA2* knockdown increased apoptosis in HepG2 and HUH6 cells (Figure S4C,S4D).

In order to explore whether *PRKAA2* can also promote HB cell proliferation *in vivo*, we conducted tumor formation experiments in nude mice. We selected si*PRKAA2*-2 because the efficiency of si*PRKAA2*-2 was better than si*PRKAA2*-1, and designed and synthesized *PRKAA2*-knockdown lentiviral plasmids with this sequence. Male nude mice at the age of 4 weeks were injected with 1×10^7 shNC and sh*PRKAA2* cells into the left and right upper groins, respectively. The tumor volume was measured for the first time 7 and 10 days after injection, and then was measured every 5 days thereafter. After 25 days, the tumor was removed, weighed and photographed, and the tumor growth curve was drawn. The weight and volume of transplanted tumors were significantly reduced after *PRKAA2* knockdown, indicating that *PRKAA2* knockdown can significantly inhibit the growth of HB tumors *in vivo* (*Figure 3H-3J*).

To further explore the role of *PRKAA2* in HB procession, BODIPY-C11 probe, which can precisely detect ferroptosis by counting the quantity of lipid peroxides in cellular membranes, was employed to detect ferroptosis. *PRKAA2* silencing increased lipid peroxide levels, indicating an increase in ferroptosis (*Figure 4A*,*4B*). The analysis of MDA (*Figure 4C*), GSH/GSSG ratio (*Figure 4D*), and iron concentration (*Figure 4E*) also proved that *PRKAA2* knockdown increased ferroptosis. We further confirmed that the cell viability after knockdown of *PRKAA2* in HB cells could be partially rescued by Z-VAD-FMK as well as ferrostatin-1 (*Figure 4F*), which again demonstrated that knockdown of *PRKAA2* caused apoptosis as well as ferroptosis in HB cells.

PRKAA2 regulates transferrin receptor 1 (TFR1) through hypoxia-inducible factor 1α (HIF-1α)

Ferroptosis is associated with several metabolism pathways including iron metabolism, lipid metabolism and amino acid metabolism, so we examined some important genes involved in these metabolic pathways after *PRKAA2* knockdown. The results showed that the expression of TFR1 increased, while

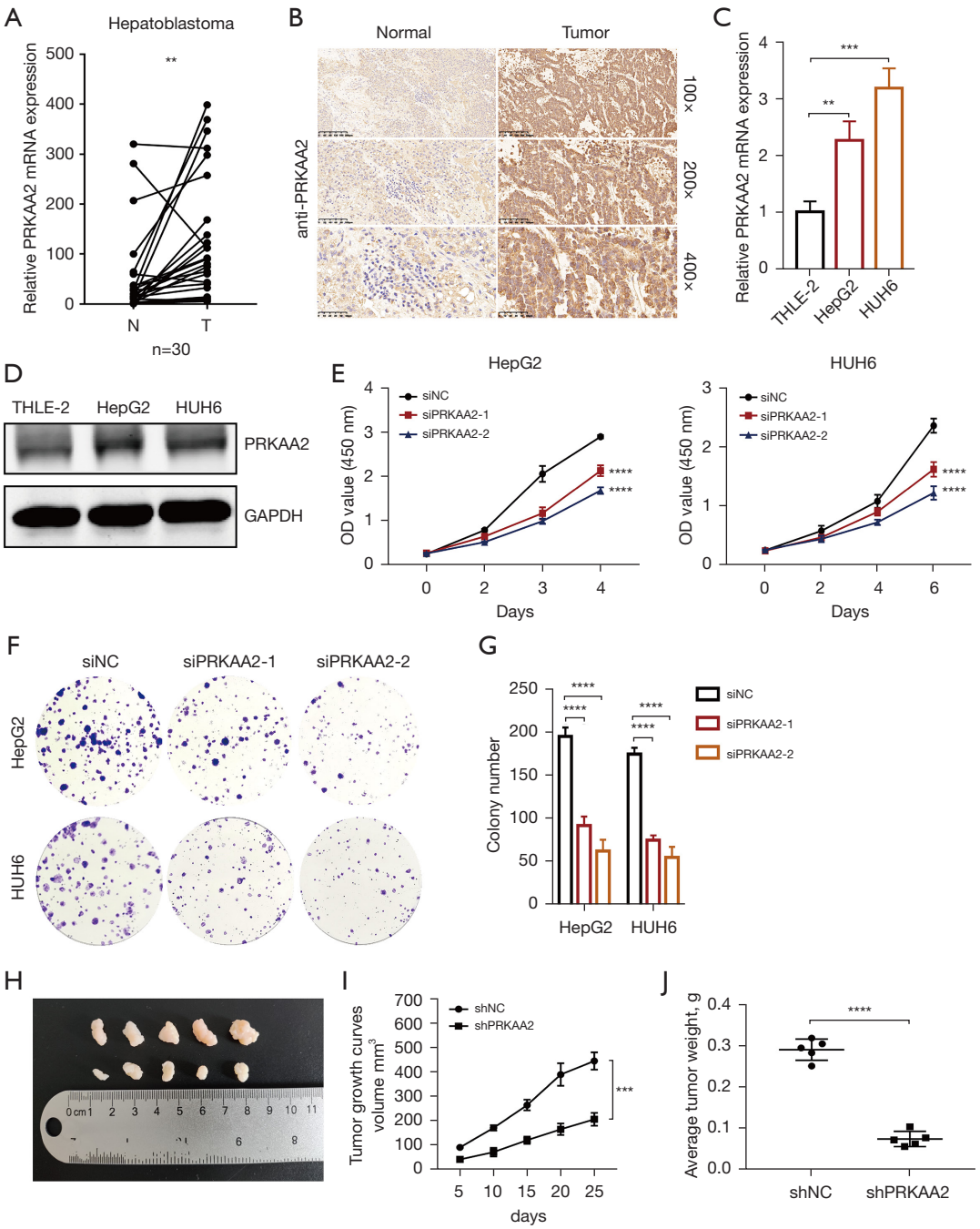

Figure 3 *PRKAA2* plays a carcinogenic role in HB. (A) Expression of *PRKAA2* mRNA in paired samples (**, P=0.003 by paired *t*-test). (B) Analysis of *PRKAA2* expression in paired samples using immunohistochemistry. Scale bar represents ×100, ×200 and ×400. (C) The mRNA level of *PRKAA2* in THLE-2, HepG2, and HUH6 was assessed. (D) The protein level of PRKAA2 in THLE-2, HepG2, and HUH6 was assessed. (E) Growth curves for HB cells following transfection with *PRKAA2* siRNA were assessed compared with controls using the CCK8 assay. (F,G) Clonogenic assay showing decreased colony formation in si*PRKAA2* HB cells compared with controls. (H) Tumors dissected from five nude mice subcutaneously injected with HUH6/shNC (up) and HUH6/sh*PRKAA2* (down) cells. Tumors were dissected after 25 days. (I) Tumor growth curves were created by graphing tumor volumes (mm^3) on the specified days. (J) Average tumor weight of nude mice (n=5 mice in each group). **, P<0.01, ***, P<0.001, and ****, P<0.0001. HB, hepatoblastoma; PRKAA2, protein kinase AMP-activated catalytic subunit alpha 2; CCK8, cell counting kit-8.

Table 3 The clinical information and pathological characteristics of 30 hepatoblastoma patients

Variable	n
Sex	
Male/female	15/15
Age at diagnosis (months)	
≥24/<24	10/20
AFP at diagnosis (ng/mL)	
≥1,200/<1,200	25/5
AFP at final detection (ng/mL)	
≥5/<5/NA	15/7/8
PRETEXT	
I-II/III-IV/NAv	16/9/5
Histology	
MIX/E/NA	14/9/7
Tumor size (cm^3)	
≥500/<500	16/14
Distant metastasis	
Yes/no	9/21
Vascular involvement	
Yes/no	17/13
Tumor rupture	
Yes/no	4/26
Multifocality	
Yes/no	6/24
Extrahepatic spread	
Yes/no	3/27
Caudate involvement	
Yes/no	13/17

AFP, alpha-fetoprotein; NA, unknown; MIX, mixed epithelial and mesenchymal; E, epithelial.

ferritin heavy chain 1 (*FTH1*), divalent metal transporter 1 (*DMT1*), ferroportin (*FPN*), recombinant solute carrier family 7, member 11 (*SLC7A11*) were no significant change (Figure S5A). TFR1 can transport Fe^{2+} into cells by binding transferrin (TF), which is the main way for Fe^{2+} to enter cells (34). The increase of TFR1 may be the reason for the increase of intracellular iron concentration. These results suggest that *PRKAA2* knockdown's ferroptosis induction may be achieved by increasing *TFR1* expression to increase intracellular iron concentration in some way. Of course, there are many genes involved that we have not tested, and it is possible that *PRKAA2* acts in other ways, too.

Since *PRKAA2* knockdown significantly increased the RNA expression of *TFR1*, we examined whether protein expression was also increased. Consistently, *PRKAA2* knockdown enhances the protein expression of TFR1 (*Figure 5A*). TFR1 expressions are delicately regulated at many levels. *IRP1* and *IRP2* control the post-transcriptional regulation of the *TFR* gene (35), while the transcription of *TFR1* gene can be induced by hypoxia-inducible factors (*HIFs*) (36). Therefore, we considered that *PRKAA2* may regulate *TFR1* expression through *IRPs* or *HIFs*. The RNA expression of *HIF-1α* was up-regulated by *PRKAA2* knockdown, and the RNA expression of *HIF-2α*, *IRP1* and *IRP2* were no change (*Figure 5B*). And the results of western blotting were consistent with those of qRT-PCR, *PRKAA2* knock down increased *HIF-1α* expression (*Figure 5C*). So, we next tried to find out whether the changes in *TFR1* expression were related to *HIF-1α* by inhibiting the up-regulation of *HIF-1α*. The treatment of the *PRKAA2* knockdown cells with *HIF-1α* inhibitor HIF-1α IN 2 reduced the elevation of *TFR1* (*Figure 5D*). This suggests that *PRKAA2* regulates *TFR1* indirectly through *HIF-1α*. Moreover, HIF-1α IN 2 reduced ferroptosis caused by *PRKAA2* knockdown (*Figure 5E,5F*, and Figure S5B,S5C). We also examined the intracellular iron concentration and found that the use of HIF-1α IN 2 also inhibited the increase of iron concentration (Figure S5D). These confirmed the effect of *PRKAA2* to negatively modulates ferroptosis by targeting *TFR1* through *HIF-1α*.

Discussion

In recent years, ferroptosis has attracted a great deal of interest in cancer research. Ferroptosis holds great potential for cancer therapy, for example, LY294002, sirolimus, and wortmannin, among other possible anti-ovarian cancer small molecule medicines, induce ferroptosis, which may lead to the development of new therapeutic alternatives for the treatment of ovarian cancer (37). Cytoglobin (CYGB) is a regulator of ROS, which can promote lipid peroxidation on the cell membrane and is a therapeutic target for colorectal cancer (38). Few researches have looked at ferroptosis in HB cells, despite the fact that it is intimately associated to carcinogenesis and development. Liu *et al.* demonstrated that m6A modification in HB enhanced

Table 4 The correlation analysis of *PRKAA2* RNA expression level and the clinical information and pathological characteristics of 30 hepatoblastoma patients

Hepatoblastoma (n=30)	*PRKAA2* expression		P value
	Low	High	
Sex			0.715
Male	9	6	
Female	7	8	
Age at diagnosis (months)			>0.999
≥24	5	5	
<24	10	10	
AFP at diagnosis			0.330
≥1,200 ng/mL	11	14	
<1,200 ng/mL	4	1	
AFP at final detection			0.634
≥5 ng/mL	6	9	
<5 ng/mL	4	3	
NA	5	3	
PRETEXT			0.021
I–II	11	5	
III–IV	1	8	
NA	3	2	
Histology			>0.999
MIX	7	7	
E	4	5	
NA	4	3	
Tumor size (cm^3)			0.715
≥500	7	9	
<500	8	6	
Distant metastasis			0.427
Yes	3	6	
No	12	9	
Vascular involvement			0.462
Yes	7	10	
No	8	5	
Tumor rupture			0.598
Yes	1	3	
No	14	12	
Multifocality			0.169
Yes	1	5	
No	14	10	
Extrahepatic spread			>0.999
Yes	2	1	
No	13	14	
Caudate involvement			0.139
Yes	4	9	
No	11	6	

PRKAA2, protein kinase AMP-activated catalytic subunit alpha 2; AFP, alpha-fetoprotein; NA, unknown; MIX, mixed epithelial and mesenchymal; E, epithelial.

HB ferroptosis resistance of SLC7A11, suggesting the immense potential of ferroptosis in HB treatment (39). Studies on HB pathogenesis have mainly focused on the WNT signaling pathway (40), but lack of further research. Investigating the ferroptosis-related markers of HB is of great significance. Mechanistic studies can provide clues for HB novel therapeutic target in the future.

Based on transcription data, bioinformatics-based analysis, expression analysis, and functional verification of DE-FRGs was conducted. Three candidate genes, including *PRKAA2*, *TRIB2*, and *GLS2*, were selected using LASSO regression and SVM-RFE, and they had strong diagnostic efficiency. *PRKAA2* significantly affected the proliferation of HB cells, according to functional verification. *PRKAA2* is the catalytic component of AMP-activated protein kinase (*AMPK*), which has complex functions and is an important regulator of energy homeostasis. *AMPK* maintains the operation of cell physiological activities and participates in a variety of signal transduction pathways (41).

Whether *AMPK* acts as a tumor suppressor or promoter may depend on the context. *AMPK* was identified as a tumor suppressor in several studies. For example, dysregulation of *AMPK* leads to dysphosphorylation of acetyl-CoA carboxylase, which accelerates hepatocellular carcinoma (42). However, there are many other studies suggested that *AMPK* promotes tumor development. Loss of either *PRKAA1* or *PRKAA2*, or both, in non-small cell lung cancer increased the tumour burden and reduced tumour-free survival (43).

Table 5 The correlation analysis of PRKAA2 protein expression level and the clinical information and pathological characteristics of 30 hepatoblastoma patients

Hepatoblastoma (n=30)	PRKAA2 expression		P value
	Low	High	
Sex			0.466
Male	9	6	
Female	6	9	
Age at diagnosis (months)			0.700
≥24	4	6	
<24	11	9	
AFP at diagnosis			0.042
≥1,200 ng/mL	10	15	
<1,200 ng/mL	5	0	
AFP at final detection			>0.999
≥5 ng/mL	7	8	
<5 ng/mL	4	3	
NA	4	4	
PRETEXT			0.007
I–II	10	6	
III–IV	1	8	
NA	4	1	
Histology			0.805
MIX	6	8	
E	5	4	
NA	4	3	
Tumor size (cm^3)			0.272
≥500	6	10	
<500	9	5	
Distant metastasis			0.014
Yes	1	8	
No	14	7	
Vascular involvement			0.139
Yes	6	11	
No	9	4	
Tumor rupture			0.598
Yes	1	3	
No	14	12	
Multifocality			0.017
Yes	0	6	
No	15	9	
Extrahepatic spread			>0.999
Yes	1	2	
No	14	13	
Caudate involvement			0.139
Yes	4	9	
No	11	6	

PRKAA2, protein kinase AMP-activated catalytic subunit alpha 2; AFP, alpha-fetoprotein; NA, unknown; MIX, mixed epithelial and mesenchymal; E, epithelial.

According to the literature review on *AMPK* and tumor by Vara-Ciruelos *et al.*, *AMPK* acts as a tumor suppressor before tumorigenesis; however, after tumor formation, *AMPK* transforms into a tumor promoting factor and plays a protective role on tumor cells (44).

In our study, *PRKAA2* appears to be a tumor-promoting factor in HB. The results of this research indicate that *PRKAA2* is a tumor-promoting factor in HB. In addition to inhibiting proliferation, *PRKAA2* inhibits ferroptosis, and knockdown of *PRKAA2* increases ferroptosis in HB cells. Therefore, abnormally elevated *PRKAA2* may inhibit the ferroptosis in HB cells, thereby promoting progression of HB. *AMPK* dysregulation may be a potential barrier to cancer treatment. Mechanistically, our results indicated that the regulation of intracellular iron concentration may be the cause of abnormal ferroptosis in HB cells. Although this has not been reported in tumors, studies have shown that iron deposition in vascular dementia is related to the upregulation of *TFR1* and *AMPK* (45). *TFR1* expressions are delicately regulated at many levels. *TFR* gene post-transcriptional regulation is regulated by *IRP1* and *IRP2* (35). Besides cellular iron, *IRP* activities can be regulated by some iron-independent effectors such as inflammation (46), oxidative stress (47), and hypoxia (48). The transcription of *TFR1* gene can be induced by *HIFs* (36). In this study, we found *PRKAA2* targets *TFR1* through *HIF-1α*, but how *PRKAA2* regulates *HIF-1α* needs further study.

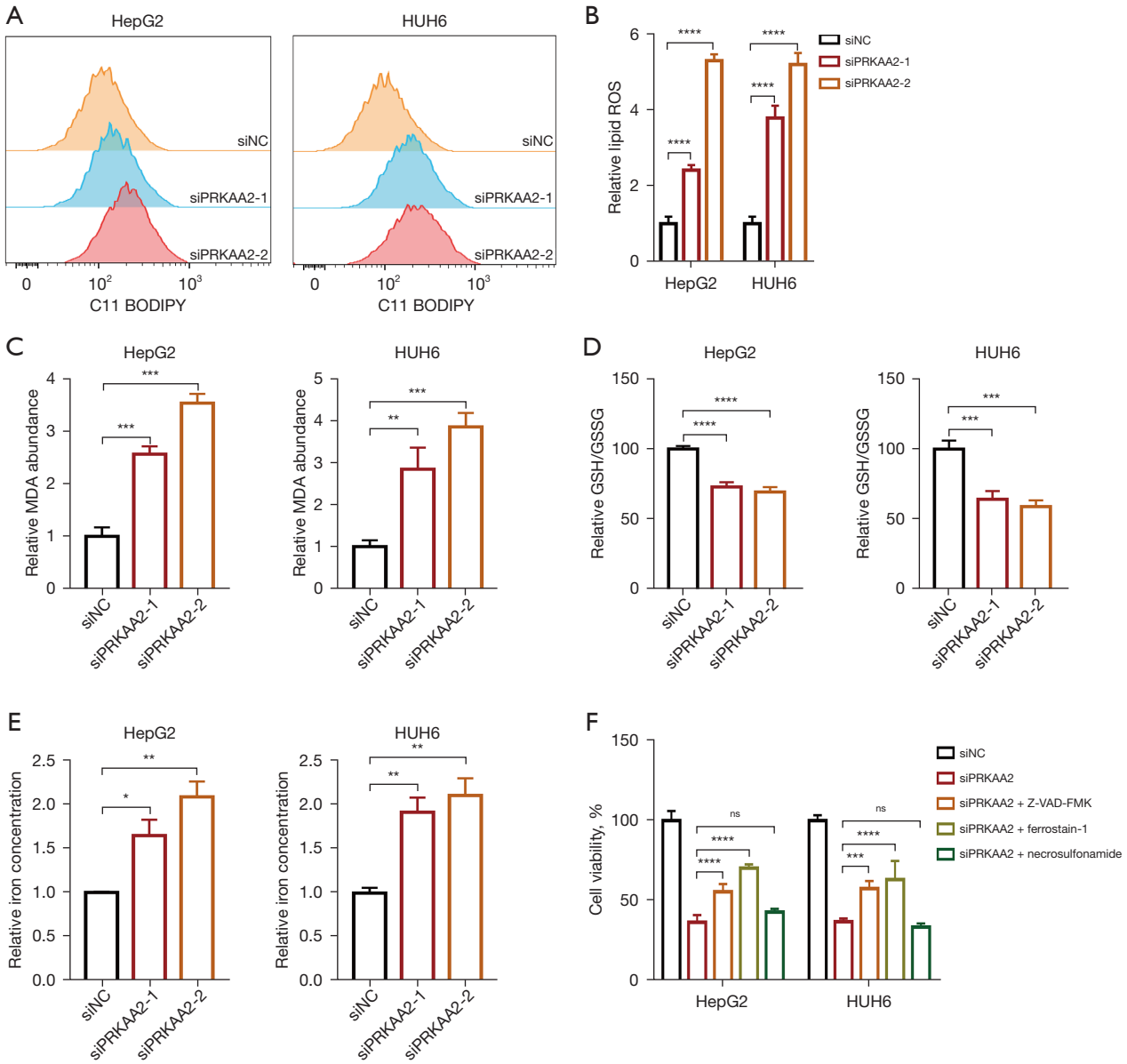

Figure 4 *PRKAA2* plays a carcinogenic role in HB through ferroptosis. (A,B) The level of lipid ROS in HB cells with *PRKAA2* knockdown compared with controls was measured via BODIPY C11 staining coupled with flow cytometry. (C) The relative MDA concentration, which were transfected with *PRKAA2* siRNA, were detected using lipid peroxidation assay kits. (D) The relative GSH/GSSG ratio, which were transfected with *PRKAA2* siRNAs, was detected using GSH and GSSG assay kits. (E) The relative iron concentration, which were transfected with *PRKAA2* siRNAs, were detected using iron assay kits. (F) Cell viability measurement following treatment with si*PRKAA2*-2 in the absence or presence of ferrostatin-1 (2 μM), Z-VAD-FMK (10 μM), or necrosulfonamide (0.5 μM) for 24 h. *, P<0.05, **, P<0.01, ***, P<0.001, and ****, P<0.0001. ns, no significant difference; HB, hepatoblastoma; PRKAA2, protein kinase AMP-activated catalytic subunit alpha 2; ROS, reactive oxygen species; MDA, malondialdehyde; GSH, glutathione; GSSG, glutathione oxidized.

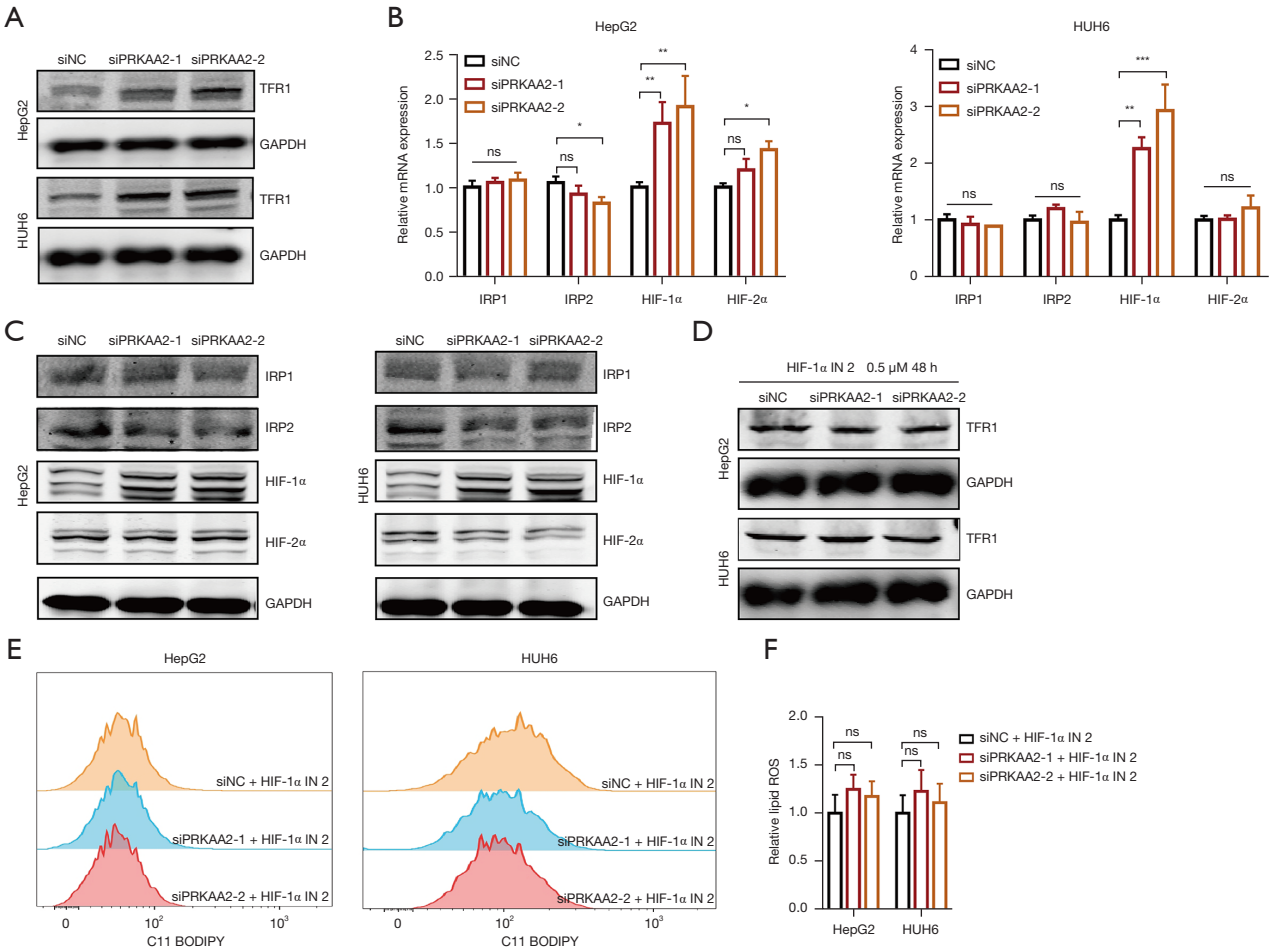

Figure 5 *PRKAA2* regulates *TFR1* through *HIF-1*α. (A) Expression of TFR1 protein in HB cells following treatment with si*PRKAA2* was measured by western blot assays. (B) Relative mRNA expression of *HIF-1*α, *HIF-2*α, *IRP1* and *IRP2* in si*PRKAA2* HB cells compared with the negative control, measured. (C) Western blot assays were used to measure the expression of HIF-1α, HIF-2α, IRP1 and IRP2 in si*PRKAA2* HB cells as well as the negative control. (D) Expression of HIF-1α and TFR1 in si*PRKAA2* HB cells as well as the negative control in the presence of HIF-1α-IN-2 (1 μM) for 48 h, measured by western blot assays. (E,F) The level of lipid ROS in HB cells with *PRKAA2* knockdown as well as controls were measured via BODIPY C11 staining coupled with flow cytometry after treatment with HIF-1α-IN-2 (1 μM) for 48 h. *, P<0.05, **, P<0.01 and ***, P<0.001. ns, no significant difference; HB, hepatoblastoma; PRKAA2, protein kinase AMP-activated catalytic subunit alpha 2; TFR1, transferrin receptor 1; HIF-1α and HIF-2α, hypoxia-inducible factor 1α and 2α; IRP1 and IRP2, Iron-regulatory proteins 1 and 2; ROS, reactive oxygen species.

Our results indicate that *PRKAA2* expression can reflect the progress of HB and are significantly correlated with prognostic factors. The protein level of PRKAA2 is significantly correlated with serum AFP level at the time of diagnosis (P=0.042), PRETEXT stage (P=0.007), distant metastasis (P=0.014) and multifocality (P=0.017) in HB patients (*Table 5*). It is very interesting that all 5 cases whose AFP levels were less than 1,200 ng/mL showed low PRKAA2 level. We provide detail about the five patients as Appendix 1. It has been reported that HB patients with an AFP <100 ng/mL had poor prognoses (4). The AFP values of these five patients were all higher than 100 ng/mL, and these 5 patients had no poor prognostic indicator such as PRETEXT stage IV, metastasis and multiple foci of the primary tumor. We hypothesized that low *PRKAA2* expression accompanied by low AFP level (1,200 ng/mL > AFP >100 ng/mL) might be a good prognostic factor. However, this needs to be verified by further expanding

the sample size. Overall, *PRKAA2* expression may be an important prognostic factor for HB.

Ferroptosis is reported to have a strong connection to the immune system (49). Cancer immunotherapy offers cancer patients fresh hope since it works via a different mechanism than conventional radiotherapy, chemotherapy or targeted therapy. In this study, we also discovered some hints that FRGs may influence the degree of HB immune infiltration. This work may serve to provide a fresh light on the molecular processes behind the origin and progression of HB as well as the investigation of prospective targeted treatments for HB, even if the hypothesis needs further clarity. Neutrophils was found to have a lower proportion in tumor samples than controls and negatively correlated with the level of *PRKAA2* (Figure S2A). Neutrophils make up a major proportion of leukocytes in the circulation and are key effector cells against cancer, may participate in cellular networks that promote antitumor resistance and mediate antitumor responses by directly destroying tumor cells (50). The role of neutrophils in HB progression and their relationship with *PRKAA2* warrant further investigation.

Our research is not exhaustive and has some limitations, for example, the sample size included in this study was not large. What's more, the mechanism of *PRKAA2* regulating ferroptosis deserves further study. In conclusion, we provide the first proof that *PRKAA2* regulates ferroptosis in HB and is a potential diagnostic and prognostic marker for HB. Our study provides some clues for the study of ferroptosis in HB, and further research may lead to novel and less aggressive therapeutic modalities for HB.

Conclusions

FRGs might play vital roles in HB development. In HB tissues, the expression of *PRKAA2* is significantly up-regulated, and *PRKAA2* greater expression is correlated with PRETEXT stage. *PRKAA2* functions as a tumor-promoting factor in HB by promoting cell proliferation and prohibiting ferroptosis. Ferroptosis-related genes *PRKAA2* is a potential diagnostic and prognostic markers for HB and could serve as a novel therapeutic target in the future.

Acknowledgments

We would like to thank all editors and reviewers for their useful feedback that improved this paper.

Funding: This work was supported by the National Natural Science Foundation of China (Nos. 81871727, 82072375, 82172357), the Major Project of Shanghai Science and Technology Innovation Action Plan (No. 22JC1402300), Shanghai Key Laboratory of Clinical Molecular Diagnostics for Pediatrics (No. 20dz2260900), Three-Year Action Plan of Shanghai Shenkang Hospital Development Center (No. SHDC2020CR2061B), Joint Project of Pudong New Area Municipal Health Commission of Shanghai (No. PW2019D-10), the Science and Technology Development Fund of Pudong New Area of Shanghai (No. PKJ2019-Y11), Clinical Project of Shanghai Municipal Health Commission (No. 20214Y0153), Shanghai "Rising Stars of Medical Talent" Youth Development Program (No. SHWRS(2020)087) and Interdisciplinary Program of Shanghai Jiao Tong University (No. YG2022QN092).

Footnote

Reporting Checklist: The authors have completed the ARRIVE reporting checklist. Available at https://jgo.amegroups.com/article/view/10.21037/jgo-23-110/rc

Data Sharing Statement: Available at https://jgo.amegroups.com/article/view/10.21037/jgo-23-110/dss

Peer Review File: Available at https://jgo.amegroups.com/article/view/10.21037/jgo-23-110/prf

Conflicts of Interest: All authors have completed the ICMJE uniform disclosure form (available at https://jgo.amegroups.com/article/view/10.21037/jgo-23-110/coif). The authors have no conflicts of interest to declare.

Ethical Statement: The authors are accountable for all aspects of the work in ensuring that questions related to the accuracy or integrity of any part of the work are appropriately investigated and resolved. The study was conducted in accordance with the Declaration of Helsinki (as revised in 2013). The study was approved by the Institutional Research Ethical Committee of Shanghai Children's Medical Centre (No. SCMCIRB-K2021076-1, 2021.10.10). All patients or their guardians provided their verbal and written consent. Experiments were performed under a project license (No. SYXK2019-0025, 2022.4.22) granted by the Shanghai Children's Medical Center, in compliance with institutional guidelines for the care and use of animals.

References

1. Czauderna P, Haeberle B, Hiyama E, et al. The Children's Hepatic tumors International Collaboration (CHIC): Novel global rare tumor database yields new prognostic factors in hepatoblastoma and becomes a research model. Eur J Cancer 2016;52:92-101.
2. Lucas B, Ravishankar S, Pateva I. Pediatric Primary Hepatic Tumors: Diagnostic Considerations. Diagnostics (Basel) 2021;11:333.
3. Feng J, Polychronidis G, Heger U, et al. Incidence trends and survival prediction of hepatoblastoma in children: a population-based study. Cancer Commun (Lond) 2019;39:62.
4. Zhi T, Zhang W, Zhang Y, et al. Clinical Characteristics and Prognosis Analysis of Infantile Hepatoblastoma-A 15-Year Retrospective Single-Center Study. Cancer Manag Res 2021;13:3201-8.
5. Fazlollahi L, Hsiao SJ, Kochhar M, et al. Malignant Rhabdoid Tumor, an Aggressive Tumor Often Misclassified as Small Cell Variant of Hepatoblastoma. Cancers (Basel) 2019;11:1992.
6. Murawski M, Weeda VB, Czauderna P. Surgical management in hepatoblastoma: points to take. Pediatr Surg Int 2023;39:81.
7. Musick SR, Smith M, Rouster AS, et al. Hepatoblastoma. 2023.
8. Stockwell BR, Friedmann Angeli JP, Bayir H, et al. Ferroptosis: A Regulated Cell Death Nexus Linking Metabolism, Redox Biology, and Disease. Cell 2017;171:273-85.
9. Dixon SJ, Lemberg KM, Lamprecht MR, et al. Ferroptosis: an iron-dependent form of nonapoptotic cell death. Cell 2012;149:1060-72.
10. Lei G, Zhuang L, Gan B. Targeting ferroptosis as a vulnerability in cancer. Nat Rev Cancer 2022;22:381-96.
11. Gao M, Monian P, Quadri N, et al. Glutaminolysis and Transferrin Regulate Ferroptosis. Mol Cell 2015;59:298-308.
12. Zhang Y, Swanda RV, Nie L, et al. mTORC1 couples cyst(e)ine availability with GPX4 protein synthesis and ferroptosis regulation. Nat Commun 2021;12:1589.
13. Li W, Fu H, Fang L, et al. Andrographolide induced ferroptosis in multiple myeloma cells by regulating the P38/Nrf2/HO-1 pathway. Arch Biochem Biophys 2023;742:109622.
14. Jennis M, Kung CP, Basu S, et al. An African-specific polymorphism in the TP53 gene impairs p53 tumor suppressor function in a mouse model. Genes Dev 2016;30:918-30.
15. Wang L, Wu S, He H, et al. CircRNA-ST6GALNAC6 increases the sensitivity of bladder cancer cells to erastin-induced ferroptosis by regulating the HSPB1/P38 axis. Lab Invest 2022;102:1323-34.
16. Ding CC, Rose J, Sun T, et al. MESH1 is a cytosolic NADPH phosphatase that regulates ferroptosis. Nat Metab 2020;2:270-7.
17. Wang W, Green M, Choi JE, et al. CD8(+) T cells regulate tumour ferroptosis during cancer immunotherapy. Nature 2019;569:270-4.
18. Ritchie ME, Phipson B, Wu D, et al. limma powers differential expression analyses for RNA-sequencing and microarray studies. Nucleic Acids Res 2015;43:e47.
19. Zhou N, Bao J. FerrDb: a manually curated resource for regulators and markers of ferroptosis and ferroptosis-disease associations. Database (Oxford) 2020;2020:baaa021.
20. Wu T, Hu E, Xu S, et al. clusterProfiler 4.0: A universal enrichment tool for interpreting omics data. Innovation (Camb) 2021;2:100141.
21. Chen B, Khodadoust MS, Liu CL, et al. Profiling Tumor Infiltrating Immune Cells with CIBERSORT. Methods Mol Biol 2018;1711:243-59.
22. Yuan JS, Reed A, Chen F, et al. Statistical analysis of real-time PCR data. BMC Bioinformatics 2006;7:85.
23. Hiyama E, Ueda Y, Kurihara S, et al. Gene expression profiling in hepatoblastoma cases of the Japanese study group for pediatric liver tumors-2 (JPLT-2) trial. Eur J Mol Cancer 2019:12-8.
24. Sumazin P, Chen Y, Treviño LR, et al. Genomic analysis of hepatoblastoma identifies distinct molecular and prognostic subgroups. Hepatology 2017;65:104-21.
25. Lin Q, Zhao Z, Liu JS. Sparse Sliced Inverse Regression Via Lasso. J Am Stat Assoc 2019;114:1726-39.
26. Sanz H, Valim C, Vegas E, et al. SVM-RFE: selection and visualization of the most relevant features through non-

linear kernels. BMC Bioinformatics 2018;19:432.
27. Liao P, Wang W, Wang W, et al. CD8(+) T cells and fatty acids orchestrate tumor ferroptosis and immunity via ACSL4. Cancer Cell 2022;40:365-378.e6.
28. Lei G, Horbath A, Li Z, et al. PKCβII-ACSL4 pathway mediating ferroptosis execution and anti-tumor immunity. Cancer Commun (Lond) 2022;42:583-6.
29. Jiang Z, Lim SO, Yan M, et al. TYRO3 induces anti-PD-1/PD-L1 therapy resistance by limiting innate immunity and tumoral ferroptosis. J Clin Invest 2021;131:e139434.
30. Hsieh CH, Hsieh HC, Shih FS, et al. An innovative NRF2 nano-modulator induces lung cancer ferroptosis and elicits an immunostimulatory tumor microenvironment. Theranostics 2021;11:7072-91.
31. Dai E, Han L, Liu J, et al. Autophagy-dependent ferroptosis drives tumor-associated macrophage polarization via release and uptake of oncogenic KRAS protein. Autophagy 2020;16:2069-83.
32. Wiernicki B, Maschalidi S, Pinney J, et al. Cancer cells dying from ferroptosis impede dendritic cell-mediated anti-tumor immunity. Nat Commun 2022;13:3676.
33. Towbin AJ, Meyers RL, Woodley H, et al. 2017 PRETEXT: radiologic staging system for primary hepatic malignancies of childhood revised for the Paediatric Hepatic International Tumour Trial (PHITT). Pediatr Radiol 2018;48:536-54.
34. Sze SCW, Zhang L, Zhang S, et al. Aberrant Transferrin and Ferritin Upregulation Elicits Iron Accumulation and Oxidative Inflammaging Causing Ferroptosis and Undermines Estradiol Biosynthesis in Aging Rat Ovaries by Upregulating NF-Kb-Activated Inducible Nitric Oxide Synthase: First Demonstration of an Intricate Mechanism. Int J Mol Sci 2022;23:12689.
35. Gammella E, Buratti P, Cairo G, et al. The transferrin receptor: the cellular iron gate. Metallomics 2017;9:1367-75.
36. Udensi UK, Tackett AJ, Byrum S, et al. Proteomics-Based Identification of Differentially Abundant Proteins from Human Keratinocytes Exposed to Arsenic Trioxide. J Proteomics Bioinform 2014;7:166-78.
37. Zhang J, Xi J, Huang P, et al. Comprehensive Analysis Identifies Potential Ferroptosis-Associated mRNA Therapeutic Targets in Ovarian Cancer. Front Med (Lausanne) 2021;8:644053.
38. Ye S, Xu M, Zhu T, et al. Cytoglobin promotes sensitivity to ferroptosis by regulating p53-YAP1 axis in colon cancer cells. J Cell Mol Med 2021;25:3300-11.
39. Liu L, He J, Sun G, et al. The N6-methyladenosine modification enhances ferroptosis resistance through inhibiting SLC7A11 mRNA deadenylation in hepatoblastoma. Clin Transl Med 2022;12:e778.
40. Zhang Y, Solinas A, Cairo S, et al. Molecular Mechanisms of Hepatoblastoma. Semin Liver Dis 2021;41:28-41.
41. Steinberg GR, Hardie DG. New insights into activation and function of the AMPK. Nat Rev Mol Cell Biol 2023;24:255-72.
42. Lally JSV, Ghoshal S, DePeralta DK, et al. Inhibition of Acetyl-CoA Carboxylase by Phosphorylation or the Inhibitor ND-654 Suppresses Lipogenesis and Hepatocellular Carcinoma. Cell Metab 2019;29:174-182.e5.
43. La Montagna M, Shi L, Magee P, et al. AMPKalpha loss promotes KRAS-mediated lung tumorigenesis. Cell Death Differ 2021;28:2673-89.
44. Vara-Ciruelos D, Russell FM, Hardie DG. The strange case of AMPK and cancer: Dr Jekyll or Mr Hyde? †. Open Biol 2019;9:190099.
45. Huo T, Jia Y, Yin C, et al. Iron dysregulation in vascular dementia: Focused on the AMPK/autophagy pathway. Brain Res Bull 2019;153:305-13.
46. Charlebois E, Fillebeen C, Katsarou A, et al. A crosstalk between hepcidin and IRE/IRP pathways controls ferroportin expression and determines serum iron levels in mice. Elife 2022;11:e81332.
47. Muto Y, Nishiyama M, Nita A, et al. Essential role of FBXL5-mediated cellular iron homeostasis in maintenance of hematopoietic stem cells. Nat Commun 2017;8:16114.
48. Anderson SA, Nizzi CP, Chang YI, et al. The IRP1-HIF-2alpha axis coordinates iron and oxygen sensing with erythropoiesis and iron absorption. Cell Metab 2013;17:282-90.
49. Wang P, Lu YQ. Ferroptosis: A Critical Moderator in the Life Cycle of Immune Cells. Front Immunol 2022;13:877634.
50. Que H, Fu Q, Lan T, et al. Tumor-associated neutrophils and neutrophil-targeted cancer therapies. Biochim Biophys Acta Rev Cancer 2022;1877:188762.

Cite this article as: Xie Y, Cui Z, Fang S, Zhu G, Zhen N, Zhu J, Mao S, Sun F, Pan Q, Ma J. Anti-ferroptotic *PRKAA2* serves as a potential diagnostic and prognostic marker for hepatoblastoma. J Gastrointest Oncol 2023;14(4):1788-1805. doi: 10.21037/jgo-23-110

Appendix 1

1. The following primer sequences were used in this study:

TFR1-F	GCTCGGCAAGTAGATGGCGATAAC
TFR1-R	ATTGTCAATGTCCCAAACGTCACC
SLC7A11-F	AGCCTGTTGTGTCCACCATCTCC
SLC7A11-R	GTCAGAGTGATGACGAAGCCAATC
PRKAA2-F	GTGAAGATCGGACACTACGTG
PRKAA2-R	CTGCCACTTTATGGCCTGTTA
18S-F	CAGCCACCCGAGATTGAGCA
18S-R	TAGTAGCGACGGGCGGTGTG
DMT1-F	TGGCTTATCTGGGCTTTGTG
DMT1-R	CACACTGGCTCTGATGGCTA
FPN-F	ACAATACGAAGGATTGACCAGT
FPN-R	ATACCAAGTTCCATCCCGAAAT
FTH1-F	GCCGAGAAACTGATGAAGCTGC
FTH1-R	GCACACTCCATTGCATTCAGCC
HIF-1α-F	CCATTAGAAAGCAGTTCCGCAAGC
HIF-1α-R	GTGGTAGTGGTGGCATTAGCAGTAG
HIF-2α-F	CCAGGGAAAAAGGAACTTGGGT
HIF-2α-R	GACCCGAAAAGAGGACGGAGA
IRP1-F	AACTGACCACATCTCCCCAG
IRP1-R	ATAGTCTGTGGTGCCTGCTT
IRP2-F	TACGGGTCTTGTTGGAAGCT
IRP2-R	ATCTGTCGGACAAGCAGGAT

2. Target sequences for siRNAs and shRNAs were as follows:
siPRKAA2-1: GUCAUCCUCAUAUUAUCAAAC
siPRKAA2-2: CAACUUUACCUGGUUGAUAAC
ShPRKAA2:CCGGGTCATCCTCATATTATCAAACCTCGAGGTTTGATAATATGAGGATGACTTTTTG

3. The following information was provided regarding the primary antibodies used in western blotting assays:
Anti-PRKAA2 antibodies (1/1000; Proteintech, 18167-1-AP, RRID:AB_10695046);
Anti-TFR1 antibodies (1/1000; Abcam, ab214039, RRID:AB_2904534);
Anti-IRP1 antibodies (1/1000; Abcam, ab183721);
Anti-IRP2 antibodies (1/1000; ABclonal, A6382, RRID:AB_2766984);
Anti-HIF-1α antibodies (1/1000; Abcam, ab179483, RRID:AB_2732807);
Anti-HIF-2α antibodies (1/1000; Abclonal, A7553, RRID:AB_2768078);
Anti-GAPDH antibodies (1/10000; Abcam, ab181602, RRID:AB_2630358)

https://dx.doi.org/10.21037/jgo-23-110

1. Detail about the five patients with low AFP level and low PRKAA2 expression

Number	AFP at Diagnosis	Age at diagnosis	PRETEXT	Histology	Tumor Size	Metastasis	Extrahepatic spread	Multifocality	Tumor rupture	Vascular involvement	Caudate involvement
1	696.4 ng/ml	11 months	I	MIX	590 cm3	NO	NO	NO	NO	NO	NO
2	943.5 ng/ml	10 months	I	MIX	448 cm3	NO	NO	NO	NO	NO	NO
3	856.9 ng/ml	31 months	II	Epithelial	643 cm3	NO	NO	NO	NO	NO	NO
4	1010.2 ng/ml	45 months	II	Epithelial	540 cm3	NO	NO	NO	YES	YES	NO
5	690.1 ng/ml	22 months	II-III	NA	252 cm3	NO	NO	NO	NO	NO	NO

2. Specific data of ΔΔCt

Pair Number	ΔΔCt=ΔCt(normalized-noncancerous)-ΔCt(normalized-Tumor)	Average ΔΔCt
1	0.187351015	0.750443124
1	0.800498056	
1	1.2634803	
2	1.555538501	1.217900169
2	0.869679343	
2	1.228482663	
3	9.25643847	8.321005907
3	8.459185325	
3	7.247393924	
4	1.157398133	1.356692126
4	1.55598612	
4	1.356692126	
5	0.53221911	0.561389829
5	0.590560547	
5	0.561389829	
6	-1.638684877	-1.316081323
6	-1.292519957	
6	-1.017039135	
7	4.111432552	3.461021244
7	4.708573759	
7	1.56305742	
8	0.471147838	-0.081526378
8	-0.497106906	
8	-0.218620067	
9	10.95563585	8.931872441
9	7.157972881	
9	8.682008593	
10	1.774275047	2.507484573
10	1.763643632	
10	3.984535039	
11	-1.193641773	-0.835490099
11	0.025653702	
11	-1.338482226	
12	0.727220454	0.424500389
12	0.658794265	
12	-0.112513553	
13	-0.008552379	-0.197565551
13	0.141298434	
13	-0.725442709	
14	-2.46922674	-0.474150913
14	0.166230644	
14	0.880543357	
15	0.369754301	-0.096661473
15	0.141497274	
15	-0.801235992	
16	8.014684308	8.811174364
16	9.666180917	
16	8.752657867	
17	6.701586931	6.327822258
17	5.279048674	
17	7.002831169	
18	2.135016937	2.196510297
18	2.207521069	
18	2.246992885	
19	3.477338478	3.297944832
19	3.20062303	
19	3.215872987	
20	2.612746572	2.723212248
20	2.903221421	
20	2.653668751	
21	5.325581803	4.951347183
21	4.565270361	
21	4.963189385	
22	1.741058643	1.802038974
22	2.084580179	
22	1.580478101	
23	2.551942839	3.100305693
23	3.648668547	
23	3.100305693	
24	4.911576917	5.06152224
24	5.211467563	
24	5.06152224	
25	6.16158126	5.820394884
25	5.479208508	
25	5.820394884	
26	4.064519051	3.844358365
26	3.62419768	
26	3.844358365	
27	8.120304956	8.312927469
27	7.891600494	
27	8.926876957	
28	4.077108354	5.483701346
28	6.631571714	
28	5.742423971	
29	2.744173446	2.183797763
29	1.551523796	
29	2.255696047	
30	8.161786668	7.690549381
30	7.725493653	
30	7.184367824	

https://dx.doi.org/10.21037/jgo-23-110

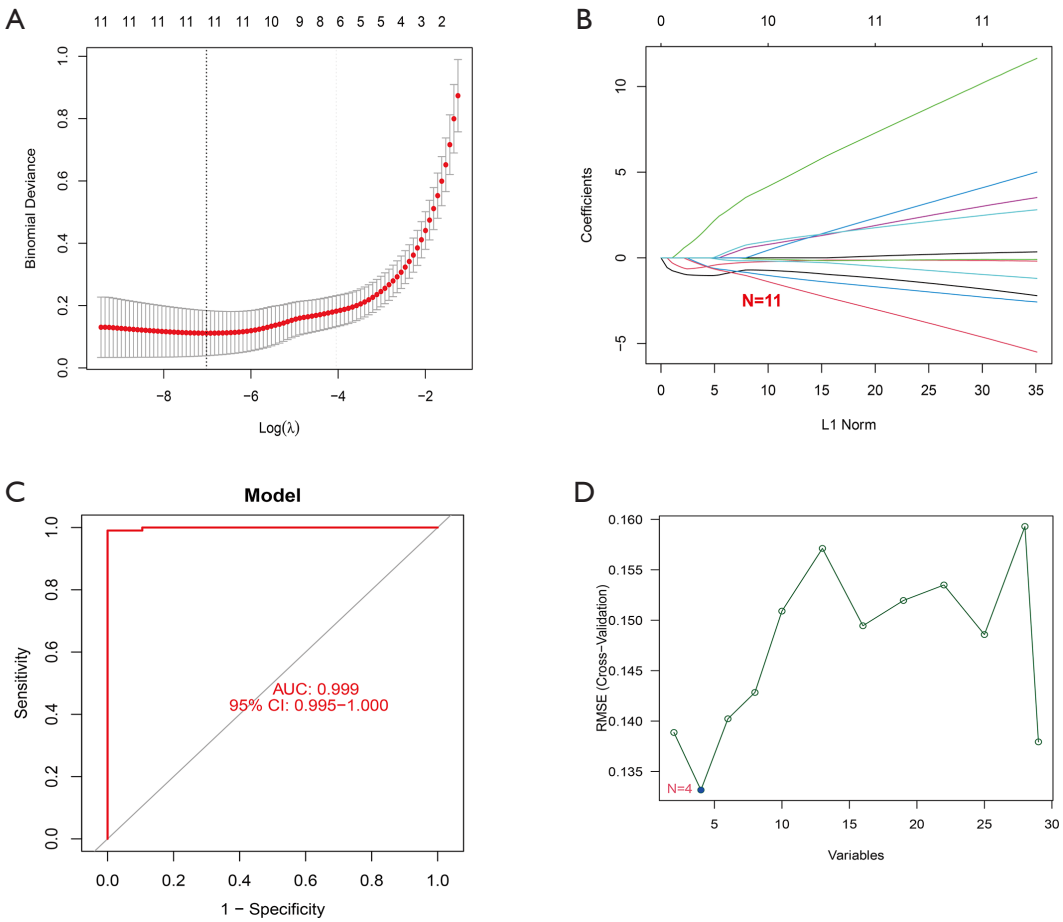

Figure S1 Selection of diagnosis marker candidates for HB by two algorithms. (A) and (B) Eleven gene expression signatures based on ferroptosis-related clusters were selected using the LASSO Cox model. (C) and (D) A visual representation of the SVM-RFE biological marker screening process. HB, hepatoblastoma; LASSO, least absolute shrinkage and selection operator; SVM-REF, support vector machine recursive feature elimination.

https://dx.doi.org/10.21037/jgo-23-110

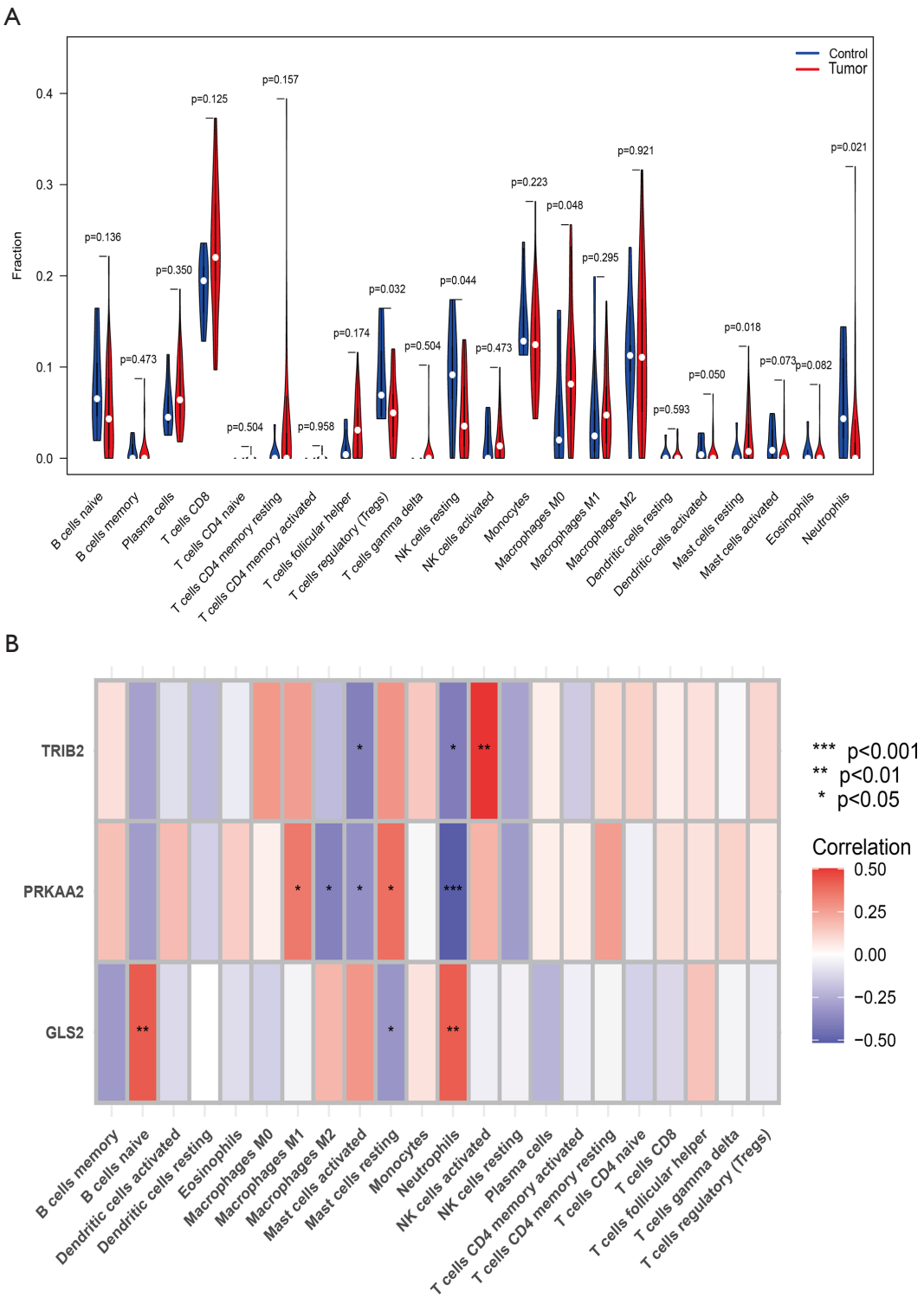

Figure S2 Analysis of immune infiltration level. (A) The differences in immunocytes' structural makeup between HB and noncancerous liver samples. Names of 22 types of infiltrating immune cells are shown in the bottom of the graph. (B) Correlation between 22 immune infiltration cells and three key genes. Gene names are on the left of the graph. *, P<0.05, **, P<0.01, and ***, P<0.001. The gradual colour change from red to blue indicates the changing process from positive correlation to negative correlation. HB, hepatoblastoma; PRKAA2, protein kinase AMP-activated catalytic subunit alpha 2; TRIB2, tribbles homolog 2; GLS2, liver-type glutaminase.

https://dx.doi.org/10.21037/jgo-23-110

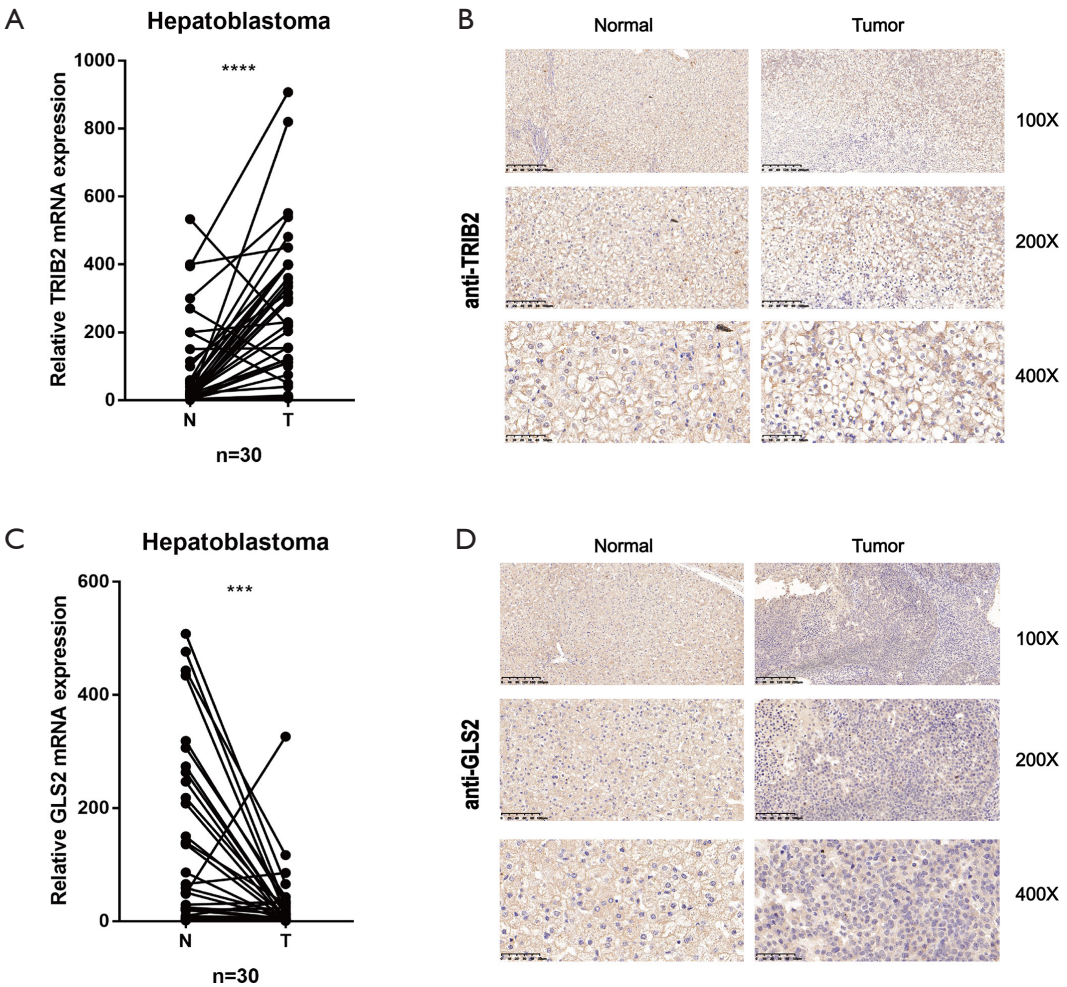

Figure S3 Expression of TRIB2 and GLS2 in paired samples. (A) Expression of TRIB2 mRNA in paired samples (****, $P<0.0001$ by paired *t*-test). (B) Analysis of TRIB2 expression in paired samples using immunohistochemistry. Scale bar represents ×100, ×200 and ×400. (C) Expression of GLS2 mRNA in paired samples (***, $P=0.0004$ by paired t-test). (D) Analysis of GLS2 expression in paired samples using immunohistochemistry. Scale bar represents ×100, ×200 and ×400. TRIB2, tribbles homolog 2; GLS2, liver-type glutaminase.

https://dx.doi.org/10.21037/jgo-23-110

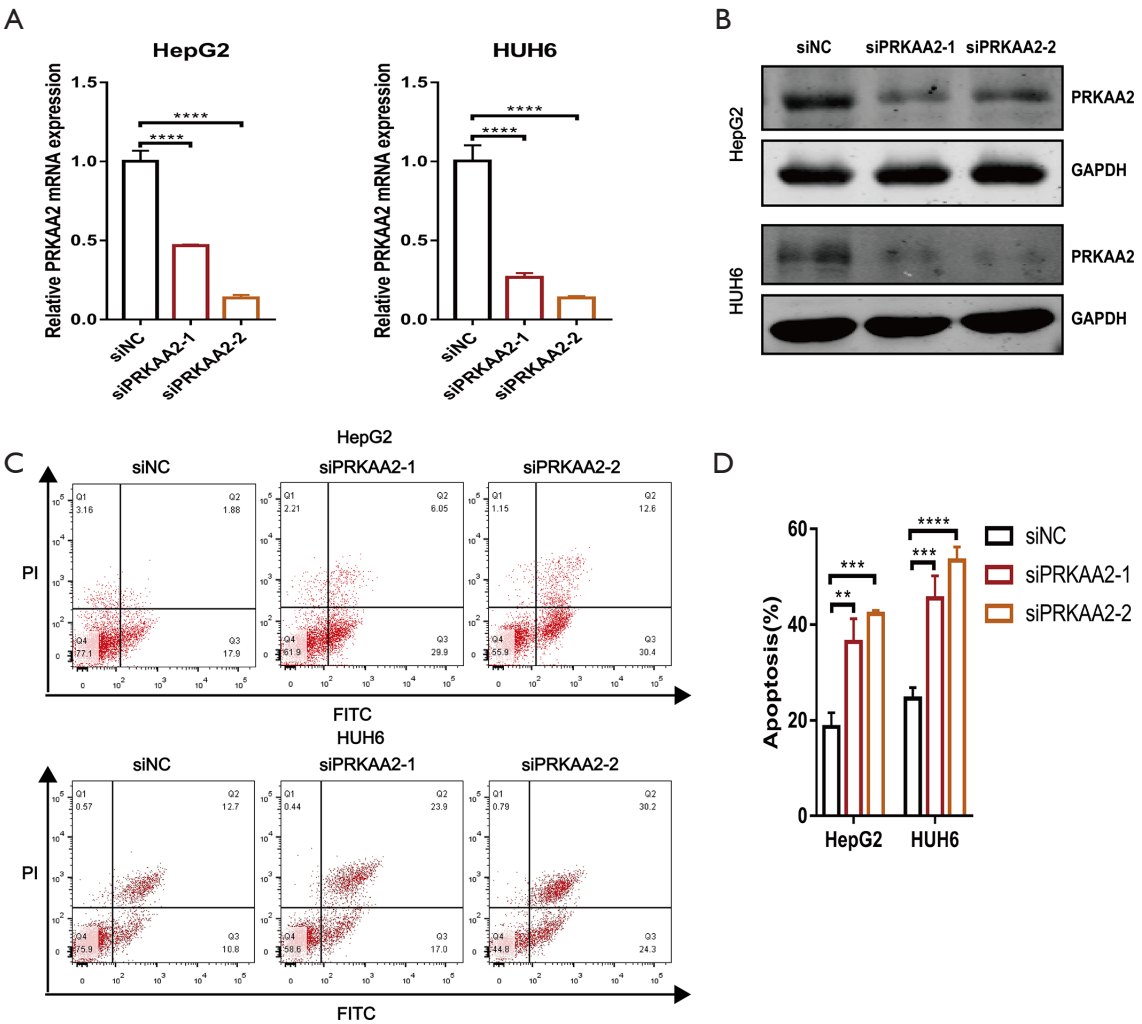

Figure S4 PRKAA2 plays a carcinogenic role in HB. (A) PRKAA2 mRNA expression in siPRKAA2 HB cells compared with the controls was measured. (****, P<0.0001 by t-test). (B) The protein level of PRKAA2 in siPRKAA2 HB cells compared with the controls was measured. (C) and (D) FACS assays were used to measure the apoptosis in HB cells with PRKAA2 knockdown compared with controls. **, P<0.01, ***, P<0.001, and ****, P<0.0001. HB, hepatoblastoma; PRKAA2, protein kinase AMP-activated catalytic subunit alpha 2.

https://dx.doi.org/10.21037/jgo-23-110

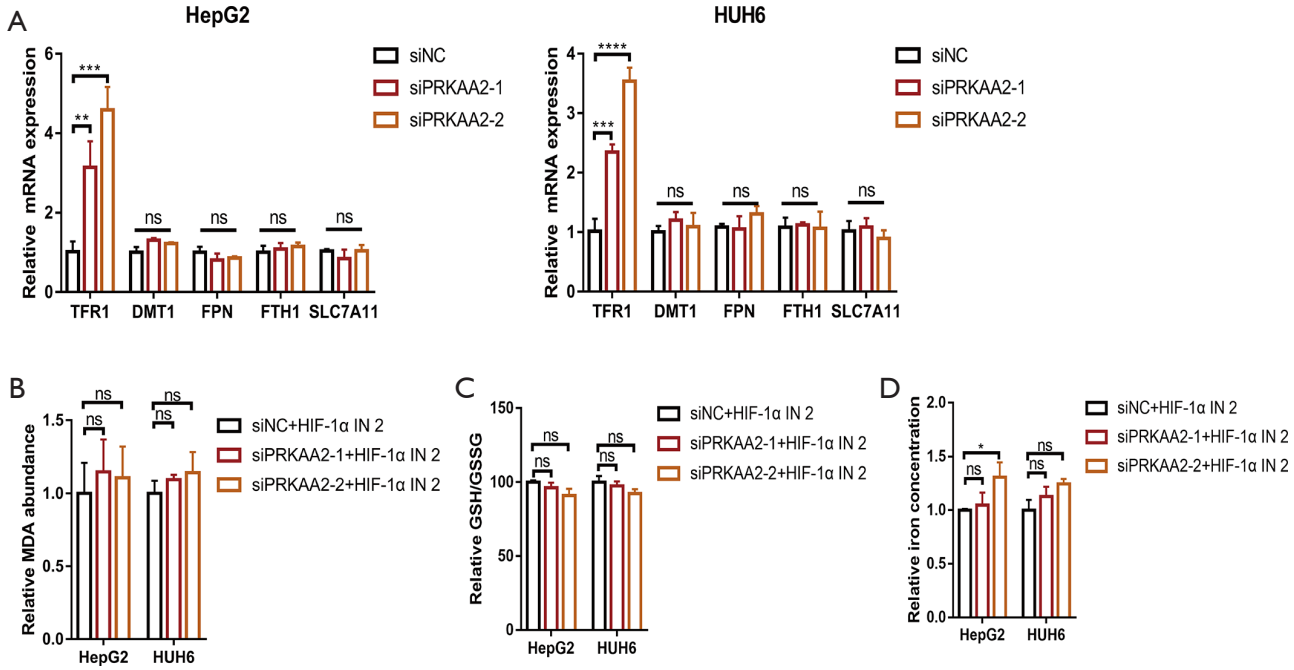

Figure S5 PRKAA2 regulates TFR1 through HIF-1α. (A) Relative mRNA expression of several genes regulating ferroptosis in siPRKAA2 HB cells compared with the controls were measured. (B-D) The relative MDA concentration (B), GSH/GSSG ratio (C) and iron concentration (D) in HB cells, which were transfected with PRKAA2 siRNA, were detected using lipid peroxidation assay kits, GSH and GSSG assay kits and iron assay kits respectively after treatment with HIF-1α-IN-2 (1 μM) for 48 h. * P<0.05, **, P<0.01, ***, P<0.001, and ****, P<0.0001. ns, no significant difference. PRKAA2, protein kinase AMP-activated catalytic subunit alpha 2; TFR1, transferrin receptor 1; HIF-1α, hypoxia-inducible factor 1α; MDA, malondialdehyde; GSH, glutathione; GSSG, glutathione oxidized.

https://dx.doi.org/10.21037/jgo-23-110